ESTIMATION OF SIDEFORCE, YAWING MOMENT AND ROLLING MOMENT DERIVATIVES DUE TO RATE OF YAW FOR COMPLETE AIRCRAFT AT SUBSONIC SPEEDS

1. NOTATION AND UNITS (see Sketch 1.1)

The derivative notation used is that proposed in ARC R&M 3562 (Hopkin, 1970) and described in Item No. 86021. Coefficients and aeronormalised derivatives are evaluated in aerodynamic body axes with origin at the aircraft centre of gravity and with the wing span as the characteristic length. The derivatives Y_r, N_r and L_r are often written as C_{Yr}, C_{nr} and C_{lr} in other systems of notation, but attention must be paid to the reference dimensions used. In particular, in forming C_{Yr}, C_{nr} and C_{lr} differentiation may be carried out with respect to $rb/2V$ not rb/V as implied in the Hopkin system. It is also to be noted that a constant datum value of V is employed by Hopkin.

This Item makes use of several other Items which have been produced at different times over a period of many years. Although the nomenclature in these Items is consistent for the important parameters such as stability derivatives, it involves some variation and duplication for the less significant parameters. Because of this, and to avoid repetition, the Notation given here is limited to the major quantities appearing in the main text of this Item and to quantities not appearing in other Items. When referred to the method in another Item the user should consult the Notation at the front of that particular Item before carrying out any calculations.

		SI	*British*
A	aspect ratio, b^2/S		
b	wing span	m	ft
C_{D0}	zero-lift profile drag coefficient		
ΔC_{D0f}	increment in C_{D0} due to trailing-edge flap deflection		
C_L	lift coefficient, $L/\frac{1}{2}\rho V^2 S$		
ΔC_{Lf}	increment in C_L due to trailing-edge flap deflection		
C_l	rolling moment coefficient, $\mathscr{L}/\frac{1}{2}\rho V^2 Sb$		
C_n	yawing moment coefficient, $\mathscr{N}/\frac{1}{2}\rho V^2 Sb$		
C_Y	sideforce coefficient, $Y/\frac{1}{2}\rho V^2 S$		
L	lift	N	lbf
$\mathscr{L}$	rolling moment	N m	lbf ft
L_v	rolling moment derivative due to sideslip; $L_v = (\partial \mathscr{L}/\partial v)/\frac{1}{2}\rho VSb$		
L_{v0}	value of L_v when wing $C_L = 0$		

$L_{\dot{v}}$	rolling moment derivative due to rate of change of sideslip; $L_{\dot{v}} = (\partial \mathscr{L}/\partial \dot{v})/\tfrac{1}{2}\rho S b^2$		
L_r	rolling moment derivative due to rate of yaw; $L_r = (\partial \mathscr{L}/\partial r)/\tfrac{1}{2}\rho V S b^2$		
$(\Delta L_r)_{corr}$	empirical correction added to allow for partially separated flow on wing (see Section 3.3.2)		
$\bar{l}_F'$	yawing moment tail arm; distance from moment reference centre to centre of pressure position of fin sideforce, measured parallel to longitudinal body axis	m	ft
M	Mach number		
$\mathscr{N}$	yawing moment	N m	lbf ft
N_v	yawing moment derivative due to sideslip; $N_v = (\partial \mathscr{N}/\partial v)/\tfrac{1}{2}\rho V S b$		
$N_{\dot{v}}$	yawing moment derivative due to rate of change of sideslip; $N_{\dot{v}} = (\partial \mathscr{N}/\partial \dot{v})/\tfrac{1}{2}\rho S b^2$		
N_r	yawing moment derivative due to rate of yaw; $N_r = (\partial \mathscr{N}/\partial r)/\tfrac{1}{2}\rho V S b^2$		
r	rate of yaw	rad/s	rad/s
S	wing planform area	m^2	ft^2
S_F	fin side area	m^2	ft^2
V	velocity of aircraft relative to air	m/s	ft/s
v	sideslip velocity	m/s	ft/s
$\dot{v}$	rate of change of sideslip velocity	m/s^2	ft/s^2
Y	sideforce	N	lbf
Y_v	sideforce derivative due to sideslip; $Y_v = (\partial Y/\partial v)/\tfrac{1}{2}\rho V S$		
$Y_{\dot{v}}$	sideforce derivative due to rate of change of sideslip; $Y_{\dot{v}} = (\partial Y/\partial \dot{v})/\tfrac{1}{2}\rho S b$		
Y_r	sideforce derivative due to rate of yaw; $Y_r = (\partial Y/\partial r)/\tfrac{1}{2}\rho V S b$		
$\bar{z}_F'$	rolling moment tail arm; distance from moment reference centre to centre of pressure position of fin sideforce, measured normal to longitudinal body axis	m	ft
α	angle of attack of longitudinal body axis	degree	degree

α_w	angle between wing zero-lift line and longitudinal body axis, so that angle of attack of wing zero-lift line is $\alpha + \alpha_w$	degree	degree
β	angle of sideslip	rad	rad
$\dot{\beta}$	rate of change of angle of sideslip	rad/s	rad/s
Λ_0	wing leading-edge sweep angle	degree	degree
$\Lambda_{1/4}$	wing quarter-chord sweep angle	degree	degree
$\Lambda_{1/2}$	wing half-chord sweep angle	degree	degree
λ	ratio of tip chord to centre-line chord (taper ratio)		
ρ	density of air	kg/m^3	slug/ft^3

Subscripts

exp	denotes experimental value
pred	denotes predicted value

Additional symbols

$(\ )_B$	denotes component due to body
$(\ )_F$	denotes component due to fin
$(\ )_f$	denotes component due to trailing-edge flap deployment at constant C_L
$(\ )_p$	denotes component due to wing planform in fully-attached flow
$(\ )_W$	denotes total component due to wing
$(\ )_\Gamma$	denotes component due to wing dihedral
$(\ )_\varepsilon$	denotes component due to wing twist
$'$	as in L_r' and L_v' denotes values in fully-attached flow
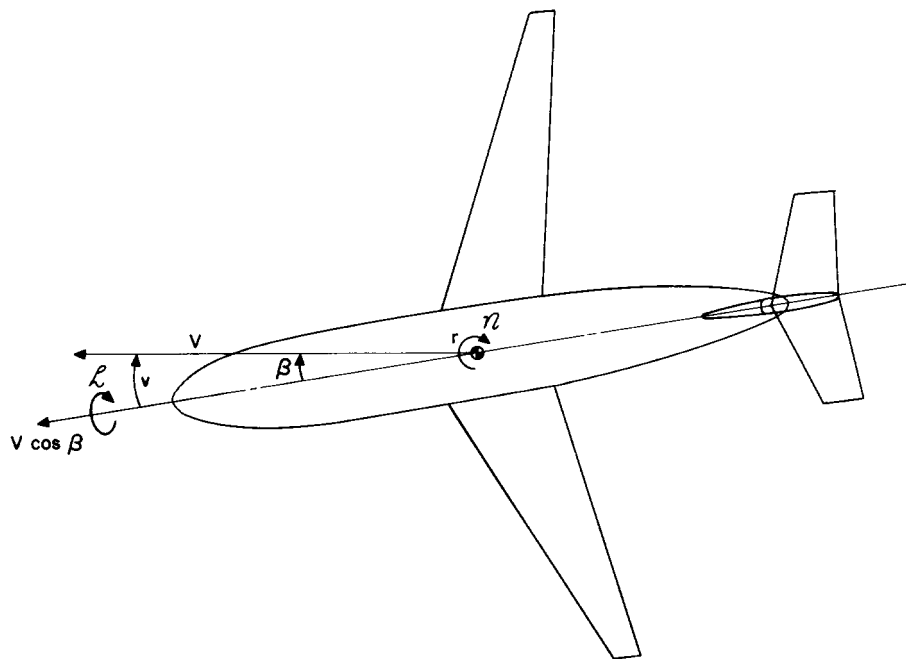
⊕ Centre of gravity position
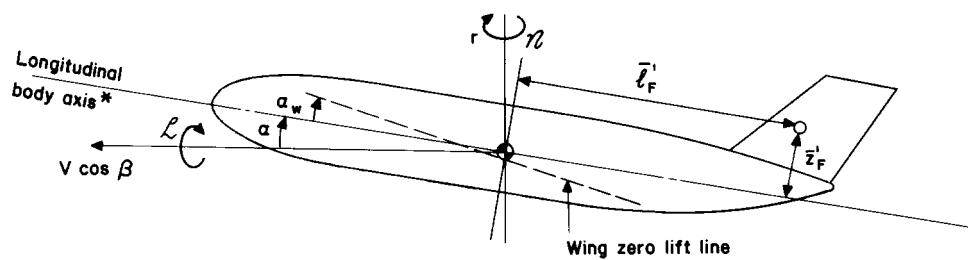
⊙ Centre of pressure position of fin sideforce

Sketch 1.1   Sign conventions

---

* The longitudinal body axis is a reference axis, fixed in the body in the plane of symmetry and passing through the centre of gravity position. The exact direction of the axis in the plane of symmetry is conventionally determined by considerations of mid-body geometry.

2.   INTRODUCTION

An aircraft's sideforce, yawing moment and rolling moment derivatives due to rate of yaw, Y_r, N_r and L_r, are customarily estimated by calculating the effects of the major components of the aircraft individually and adding together the part derivatives so obtained. For aircraft at subsonic speeds, separate Items on the various part derivatives have been issued over a number of years and each of the major components is covered. This Item demonstrates how the methods in those separate Items may be combined to provide an estimate of the derivatives of a complete aircraft, and illustrates the overall accuracy of prediction by means of comparisons with wind-tunnel and flight-test data.

Tables 2.1 and 2.2 list the major components of Y_r, N_r and L_r and the Items from which they may be estimated. The total values of the derivatives are obtained by evaluating each component at the same angle of attack and summing the results. The Items that deal specifically with Y_r, N_r and L_r often require further information, such as wing lift coefficient or the lift and drag coefficient increments due to trailing-edge flap deflection. Such information may be obtained from other Items and these are also listed in the Tables. If static stability wind-tunnel data are available for the aircraft of interest then these can sometimes be used as an alternative source for the additional information required.

Comparisons between experimental and predicted values of Y_r, N_r and L_r are discussed in Section 3 in terms of magnitude and variation with angle of attack. The Derivation and References are given in Section 4.

Section 5 contains a detailed worked example that demonstrates the calculation of the component parts of the derivatives for a particular aircraft and their subsequent combination. The choice of aircraft is the same as that used to demonstrate the calculation of derivatives due to sideslip in Item Nos 81032 and 82011 (Derivations 57 and 59). The example devotes a separate subsection to the calculation of each component and describes at which stages in the calculation use is made of the additional Items listed in Tables 2.1 and 2.2 and when experimental data, if available, may be useful. As the example provides guidance and information on points that are not covered in other Items it is advisable to refer to the appropriate subsection of the example to obtain the best use of each Item dealing with the separate components of Y_r, N_r and L_r.

A simplified method for estimating complete aircraft values rapidly is given in Appendix A.

TABLE 2.1 SIDEFORCE AND YAWING MOMENT DERIVATIVES

Component	Due to	Calculated from Item No.	Possible additional Item Nos	
$(N_r)_w$	Wing[*]	71017[46]	Aero W.02.04.01[34] , 02[35] and 03[38] 76003[54] , 70011[45] 75013[53] , 74009[49] , 74011[51] , 74012[52] Aero F.01.01.08[37] and 09[36] Aero W.01.01.01[39]	for wing zero-lift drag coefficient for wing lift coefficient for lift coefficient increments due to trailing-edge flap deflection
$(N_r)_f$	Trailing-edge flap deployment (at constant C_L)	71017[46]	75013[53] , 74010[50] Aero F.02.01.06[32] and 07[31], 87024[66]	for increment in wing zero-lift drag coefficient due to trailing-edge flap deflection
$(Y_r)_B$, $(N_r)_B$	Body	83026[61]		
$(Y_r)_F$, $(N_r)_F$	Fin	82017[60]	82010[58] 70011[45] Aero C.01.01.01[40]	for fin sideforce derivative and centre of pressure position in sideslip
Item No. Aero A.07.01.00[33] gives a brief introduction to the various components of the yawing-moment stability derivatives and their related Data Items. (Derivation numbers are given as indices.)				

[*]   This component depends on the wing lift coefficient. If trailing-edge flaps are deployed the lift coefficient of the wing with flap deflected is used. It therefore includes the effect of the lift increment produced by the flap. (See Sections 5.3 and 5.4.)

TABLE 2.2 ROLLING MOMENT DERIVATIVE

Component	Due to	Calculated from Item No.	Possible additional Item Nos	
$(L_r)_W \begin{cases} (L_r)_p \\ (L_r)_\Gamma \\ (L_r)_\varepsilon \end{cases}$ Wing $\begin{cases} \text{planform}^* \\ \text{dihedral} \\ \text{twist} \end{cases}$		72021^{47}	76003^{54} , 70011^{45} $\quad$ for wing lift coefficient 75013^{53} , 74009^{49} , 74011^{51} , 74012^{52} $\quad$ for lift coefficient Aero F.01.01.08^{37} and 09^{36} $\quad$ increment due to Aero W.01.01.01^{39} $\quad$ trailing-edge flap deflection	
$(L_r)_f$	Trailing-edge flap deployment (at constant C_L)	72021^{47}	Aero C.01.01.03^{43} , 74009^{49} $\quad$ for slope of lift increment Aero F.01.01.08^{37} and 09^{36} $\quad$ curve with trailing-edge flap deflection	
$(\Delta L_r)_{corr}$	Partial separation of wing flow	This Item: Equations (3.1) and (3.2)	81032^{57} Aero A.06.01.03^{41} and 09^{42} , Aero C.01.01.01^{40} $\quad$ for predicted 73006^{48} , 80033^{55} , 80034^{56} , 82010^{58} $\quad$ value of L_v	
$(L_r)_F$	Fin	82017^{60}	82010^{58} $\quad$ for fin sideforce derivative 70011^{45} $\quad$ and centre of pressure position Aero C.01.01.01^{40} $\quad$ in sideslip	
Item No. Aero A.06.01.00^{44} gives a brief introduction to the various components of the rolling-moment stability derivatives and their related Data Items. (Derivation numbers are given as indices.)				

*   This component depends on the wing lift coefficient. If trailing-edge flaps are deployed the lift coefficient of the wing with flap deflected is used. It therefore includes the effect of the lift increment produced by the flap. (See Sections 5.3 and 5.4.)

3. COMPARISONS WITH EXPERIMENTAL DATA

3.1 Discussion of Data

The accuracy with which the methods in the Items listed in Tables 2.1 and 2.2 predict Y_r, N_r and L_r for complete aircraft has been assessed by making comparisons with the values measured in the wind-tunnel tests reported in Derivations 1 to 20 and the values extracted from flight-test results that are reported in Derivations 21 to 30. Data have been studied for a wide variety of aircraft types representing civil transport aircraft, high performance fighter aircraft and light and general aviation aircraft, together with results for a number of simpler wind-tunnel models of the type employed to study the effect of systematic variations of geometric parameters. The majority of these data have been taken from low-speed tests for clean-wing configurations with no high-lift devices deployed. Experimental data for other conditions are less abundant, but the analysis included a limited number of results from tests at high subsonic Mach numbers ($M \approx 0.8$) and a few data from low-speed tests on configurations with wing leading-edge slats or trailing-edge flaps deployed.

It should be noted that wind-tunnel data from two types of test have been used. In one type a curved flow represents the yaw rate of the aircraft and this enables the direct measurement of the rate of yaw derivatives. In the second type of test the aircraft is mounted on a forced-oscillation rig and the rate of yaw derivatives are measured only in combination with a derivative due to the rate of change of sideslip, *i.e.* these tests give $Y_r - Y_{\dot{v}}\cos\alpha$, $N_r - N_{\dot{v}}\cos\alpha$ and $L_r - L_{\dot{v}}\cos\alpha$. The $\dot{v}$ derivatives arise from the body, wing and the fin and become increasingly important as the angle of attack increases, see References 62 and 63. Reference 62 discusses the causes and magnitudes of the wing and fin contributions to the derivatives $N_{\dot{v}}$ and $L_{\dot{v}}$ in detail and concludes that they can not be estimated satisfactorily by simple means. In the case of the derivative $Y_{\dot{v}}$ the body also contributes significantly at low α (see Item No. 83026). In order to provide an indication of the practical importance of the rate of change of sideslip, data from oscillatory tests have been included in the present study and have been compared directly with the predicted rate of yaw derivatives, except in the case of $Y_{\dot{v}}$ when the slender-body theory estimate discussed in Item No. 83026
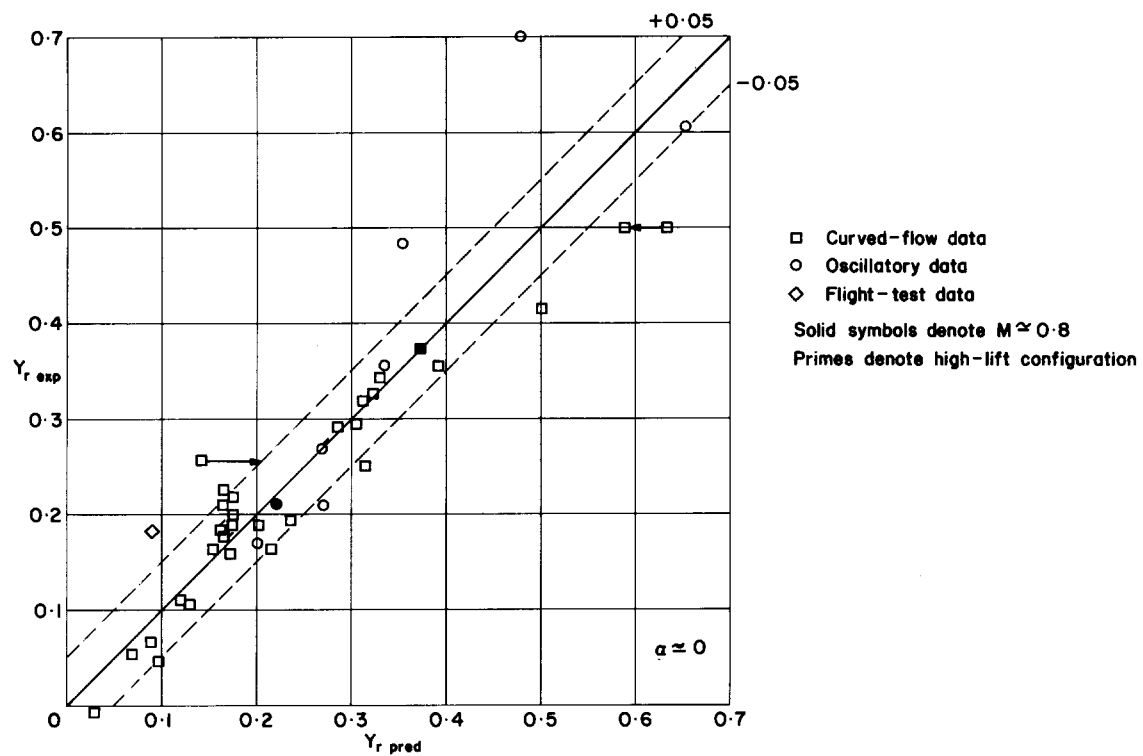
has been used. These comparisons have been confined to low values of angle of attack ($\alpha < 10°$) where the derivatives $N_{\dot{v}}$ and $L_{\dot{v}}$ should not be too large. Errors between predicted and experimental values of this second type can, however, be expected to be higher than those for curved-flow wind-tunnel data.

The flight-test data that have been used come from tests in which the dynamic response of an aircraft to various control inputs is measured and then a complete set of aerodynamic stability derivatives is deduced which corresponds to that response. The accuracy with which the various derivatives can be identified by this process depends on the sensitivity of the response of the aircraft to each derivative. Usually, satisfactory estimates of N_r and L_r can be obtained, although L_r is sometimes subject to a fairly high uncertainty. The response of an aircraft is too insensitive to Y_r for an accurate value of this derivative to be necessary and so Y_r is frequently omitted from such analyses, a point which should be remembered when examining the accuracy of prediction of Y_r in general. In the extraction of flight-test results the $\dot{v}$ derivatives are usually ignored. Reference 63 shows that they can have a significant effect on the estimated rate of yaw derivatives at high angles of attack. However, at low angles of attack ($\alpha < 10°$) they are considered to be sufficiently small to be ignored in direct comparisons between the flight-test data and the predicted values of N_r and L_r. Because of the errors involved in isolating particular derivatives from the flight-test data and the omission of the $\dot{v}$ derivatives, the errors between predicted and experimental flight-test values can be expected to be higher than for curved-flow wind-tunnel data.
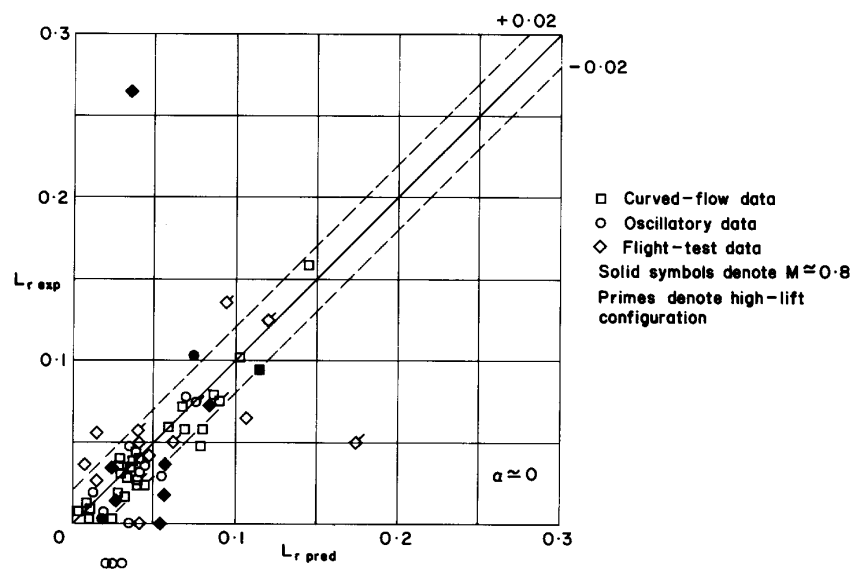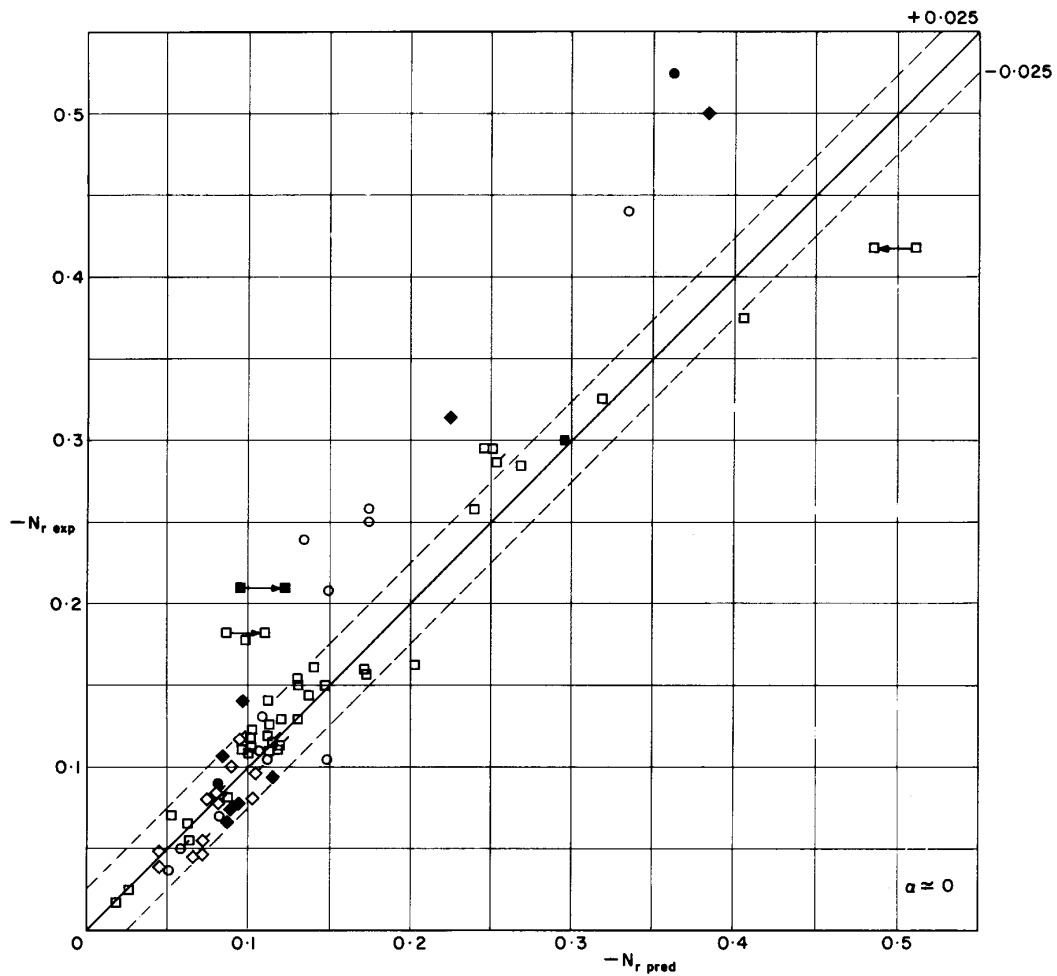
3.2 Accuracy of Prediction for $\alpha \approx 0$

The predicted and experimental values of Y_r, N_r and L_r at low angles of attack are compared in Sketches 3.1, 3.2 and 3.3. Sketch 3.1 shows that the experimental values of Y_r are generally predicted to within ± 0.05 or, at high values, to within ± 15 per cent. The prediction for the oscillatory rig data have $-(Y_{\dot{v}})_B$ added (see Section 3.1). Sketch 3.2 shows that the experimental values of N_r are generally predicted to within ± 0.025 or, at high values, to within ± 15 per cent, with poorer agreement being shown for some oscillatory rig and flight-test data. Sketch 3.3 shows that L_r is generally predicted to within ± 0.02, although there are some larger errors mainly in cases of flight-test data. Possible causes of the discrepancies in the oscillatory rig and flight-test data have been discussed in the preceding section. Overall the accuracy of prediction is consistent with the accuracy figures quoted in individual Items, approximating to the square root of the sum of the squares of the individual errors.

For those cases in Sketches 3.1 and 3.2 where curved-flow data show a large prediction error, it has been found that this can be attributed, at least in part, to errors in the fin contributions predicted by Item No. 82017. Such inaccuracies can arise if the aircraft configuration departs significantly from the simple geometries that are considered in Item Nos 82010 and Aero C.01.01.01, when those Items are used to provide estimates of the fin sideforce derivative in steady sideslip, $(Y_v)_F$, and the yawing and rolling moment tail arms $\overline{l}'_F$ and $\overline{z}'_F$ that form part of the method in Item No. 82017. However, if values of $(Y_v)_F$, $(N_v)_F$ and $(L_v)_F$ are available from wind-tunnel tests these can be compared with the predicted values to determine empirical corrections, see Section 5.6. Examples of the improvements that can be introduced by such corrections are illustrated by arrows in Sketches 3.1 and 3.2.

Sketch 3.1   Comparison of predicted and experimental Y_r

Sketch 3.2   Comparison of predicted and experimental N_r

□ Curved−flow data
○ Oscillatory data
◇ Flight−test data
Solid symbols denote M ≅ 0·8
Primes denote high−lift configuration

Sketch 3.3   Comparison of predicted and experimental L_r

3.3 Variation with α

A typical set of experimental data is used for illustration purposes throughout Sections 3.3, 3.4 and 3.5. These data have been taken from Derivations 3 and 7 which report on a number of curved-flow wind-tunnel tests of the aircraft model shown in Sketch 3.4. The data are presented as a whole in Sketches 3.5 to 3.7 and cover both the cruise (clean) configuration and the landing configuration with leading-edge slats, trailing-edge flaps and undercarriage deployed. Reference to particular features of the sketches is made where appropriate. Section 3.3 considers the effect of α without the deployment of high-lift devices, Section 3.4 the changes due to such devices and Section 3.5 the effect of Mach number. The behaviour of the derivatives is a good representation for a wide variety of aircraft configurations.

3.3.1 Sideforce and Yawing Moment Derivatives

The predicted values of Y_r and N_r vary only slightly as the angle of attack and wing lift coefficient increase. This is because the fin provides the major contributions to Y_r and N_r and these are affected only by the small variation in the effective yawing moment tail arm (see Sections 5.6 and 5.7). There is also an increase in the magnitude of the lift-dependent part of the wing contribution to N_r but this remains small compared to other components (see Sections 5.3 and 5.7). The experimental values of Y_r and N_r vary only slightly as the angle of attack increases, in agreement with the predicted values, until large departures from the low angle of attack values accompany the appearance of flow separation effects. Significant variations with angle of attack are not usually apparent until α exceeds 10°, and for highly swept wings the values of Y_r and N_r remain essentially constant up to 15° or 20°. The predicted values therefore model the experimental behaviour quite well over the initial angle of attack range. In general the experimental values of Y_r show more variation than N_r, but as Y_r is comparatively unimportant in stability calculations such variation can be neglected. The cruise-configuration data in Sketch 3.5 illustrate these points.

3.3.2 Rolling Moment Derivative

The wing planform and the fin provide the major contributions to L_r. The value predicted in Item No. 72021 for the wing planform contribution in fully-attached flow, $(L_r)_p$, is proportional to the wing C_L and varies linearly with α (see Section 5.4). The predicted contribution of the fin varies non-linearly with α because of the changes in the effective rolling moment tail arm but this is less significant (see Section 5.6). Consequently the value predicted for a complete aircraft under the assumption of fully-attached flow, L_r', increases almost linearly with α (see Section 5.7)[*]. Experimental values of L_r' depart quickly and severely from that prediction, falling well below L_r' from low values of α onwards, as demonstrated by the cruise-configuration data in Sketch 3.6a. This is due to the fact that the magnitude of the planform contribution is dramatically reduced by the occurrence of small areas of separated flow. For the same reason, the experimental planform contribution to $-L_v$ shows a very similar departure from its value in attached flow, that is also proportional to the wing C_L. Reference 64 gives a method that makes use of this similarity to produce an empirical correction term $(\Delta L_r)_{corr}$ that is added to $(L_r')_W$ to allow for the effect of partial flow separation. The method requires appropriate experimental values of L_v, and Item No. 72021 recommends that it be employed whenever such data are available.

The correction term is equal to half the difference between the value predicted for the planform contribution to L_v in attached flow and the experimental value in partially-separated flow. For an isolated plain wing this can be written

$$(\Delta L_r)_{corr} = 0.5[(L_v)_{p\,pred} - (L_v)_{W\,exp}].$$ (3.1)

---

[*] Primes as in L_r' and L_v' denote values in attached flow. Note that the planform contributions denoted by $(L_r)_p$ and $(L_v)_p$ are only defined as values in attached flow and therefore they do not carry primes.

Reference 64 presents a large number of comparisons with experimental data for a wide range of wing planforms that demonstrate that a correction of this magnitude leads to much improved estimates. It should be noted that the factor 0.5, which is empirical, must be adjusted if the parameters that are used to make L_v and L_r dimensionless are different from those in the Notation.

In most cases the experimental values of L_v that are available do not allow a direct comparison of predicted and experimental planform contributions because the wing has camber, dihedral and twist and is tested only in combination with a body or as part of a complete configuration. To allow for this Equation (3.1) is rewritten in a more general form that permits direct substitution of those data,

$$(\Delta L_r)_{corr} = 0.5[(L'_{v\ pred} - L'_{v0\ pred}) - (L_{v\ exp} - L_{v0\ exp})].$$ (3.2)

The total wing contribution to L_r is

$$(L_r)_W = (L'_r)_W + (\Delta L_r)_{corr}.$$ (3.3)

The values of L_v at zero wing C_L, L_{v0}, are included to ensure that $(\Delta L_r)_{corr}$ is zero when the planform contribution is zero. The values of L_v may be for an isolated wing, a wing-body or a complete aircraft, provided the same configuration is taken throughout. Equation (3.2) reduces precisely to Equation (3.1) only if all components of L_v, apart from the wing planform contribution, are predicted exactly. The correction obtained is therefore likely to be better when deduced from data for the simpler configurations, although a qualitative improvement will always be obtained.

Section 5.4.3 demonstrates the application of Equations (3.2) and (3.3). Estimates of the various component parts of L_v for an aircraft can be evaluated by using Item Nos Aero A.06.01.03 and 09, Aero C.01.01.01, 73006, 80033, 80034 and 82010 as described in Item No. 81032.

Sketches 3.6a and 3.6b illustrate how a major improvement in the prediction of L_r is introduced through $(\Delta L_r)_{corr}$. Sketch 3.6a shows the predicted values L_r and L'_r together with the experimental data. Sketch 3.6b compares the experimental variation of L_v with the predicted values of L'_v for the wing-body configuration, and those data have been substituted in Equation (3.2) to evaluate $(\Delta L_r)_{corr}$. The close similarity in the experimental behaviour of L_r and L_v should be noted. It is this that leads to the excellent prediction of L_r. For other aircraft this similarity is sometimes less marked, with the result that the corrected values of L_r do not always follow the experimental data quite as well as in Sketch 3.6a.

3.4 High-lift Devices

3.4.1 Sideforce and Yawing Moment Derivatives

The deployment of leading-edge slats or trailing-edge flaps has little effect on the experimental values of Y_r and N_r. Their main effect is to delay to higher angles of attack any tendency to depart from the essentially constant values maintained at low α and otherwise they cause little change in magnitude. Theoretically, (see Section 5.3.2), a small change in N_r is predicted as a result of the deployment of trailing-edge flaps and this is in reasonable agreement with the experimental data. Trailing-edge flap deployment is assumed to have no effect on the predicted values of Y_r. Sketches 3.5a and 3.5b compare some cruise and landing-configuration data to show the effect of slat and flap deployment. Overall the agreement between prediction and experiment is comparable to that achieved for aircraft without high-lift devices although the qualitative dependence on α is only partially predicted.

3.4.2 Rolling Moment Derivative

The deployment of high lift-devices has a much greater effect on L_r than on Y_r and N_r. Such devices influence the attached-flow value of the wing planform contribution by changing the wing C_L, and for trailing-edge flaps there is also a small contribution that is independent of the wing C_L (see Section 5.4.2). Furthermore, because they change the flow separation characteristics of the wing a separate calculation of $(\Delta L_r)_{corr}$ has to be made by substituting into Equation (3.2) values of L_v appropriate to the high-lift configuration (see Section 5.4.3).

Comparisons with experimental data have shown that for high-lift configurations the general accuracy of prediction of L_r at low values of α is comparable to that achieved for clean-wing configurations. As α increases the predicted values of L_r do not follow the experimental variation so closely because the corrections made with $(\Delta L_r)_{corr}$ are too small, although they still introduce a substantial improvement at high values of α.
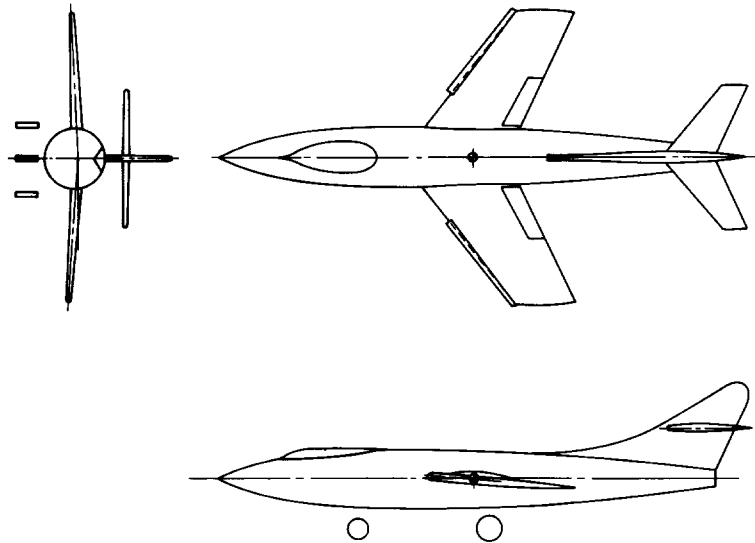
Sketches 3.6c and 3.6d show landing-configuration data that may be compared with the cruise-configuration data in Sketches 3.6a and 3.6b. The variation of the predicted values of L'_v and the experimental values of L_v are shown for the fin-off configuration in Sketch 3.6d. These have been substituted in Equation (3.2). It can be seen that, compared with the clean-wing data, the high-lift devices moderate the departure of the experimental data from L'_r and L'_v at high values of α, but that $(\Delta L_r)_{corr}$ underestimates the departure from L'_r in Sketch 3.6c.
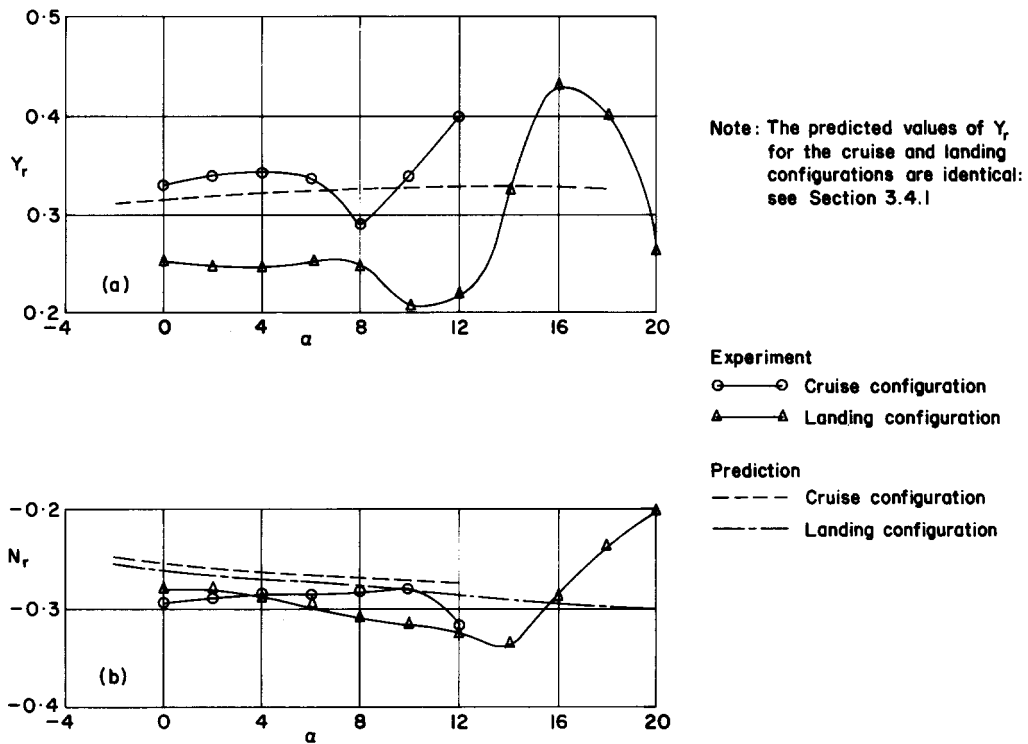
3.5 Variation with Mach Number

The effect of Mach number on the derivatives Y_r, N_r and L_r is moderate for Mach numbers up to about 0.8, the derivatives increasing slowly in magnitude. Comparisons with experimental data suggest that the theoretical methods model the effect of Mach number quite well, until the appearance of shock waves at high Mach numbers causes the experimental derivatives to depart rapidly from their low speed values. Sketch 3.7 gives an example of the experimental and predicted variations with Mach number for each of the derivatives.

### 3.6 Comparisons with Flight-test Data

Sketches 3.8a to 3.8d show four aircraft configurations for which predicted values of N_r and L_r have been compared with flight-test data. These indicate the range of aircraft geometries to which the Data Item methods can be applied. The magnitudes of the predicted components of Y_r, N_r and L_r are illustrated for cruise conditions. The general agreement with flight test data is quite good, as demonstrated in Sketch 3.9 for an aircraft with variable wing sweep from $\Lambda_0 = 26°$ to $58°$.

Sketch 3.4   Aircraft model tested in Derivations 3 and 7

Note : The predicted values of Y_r
for the cruise and landing
configurations are identical:
see Section 3.4.1

Experiment
⊖———⊖ Cruise configuration
▲———▲ Landing configuration

Prediction
— — — Cruise configuration
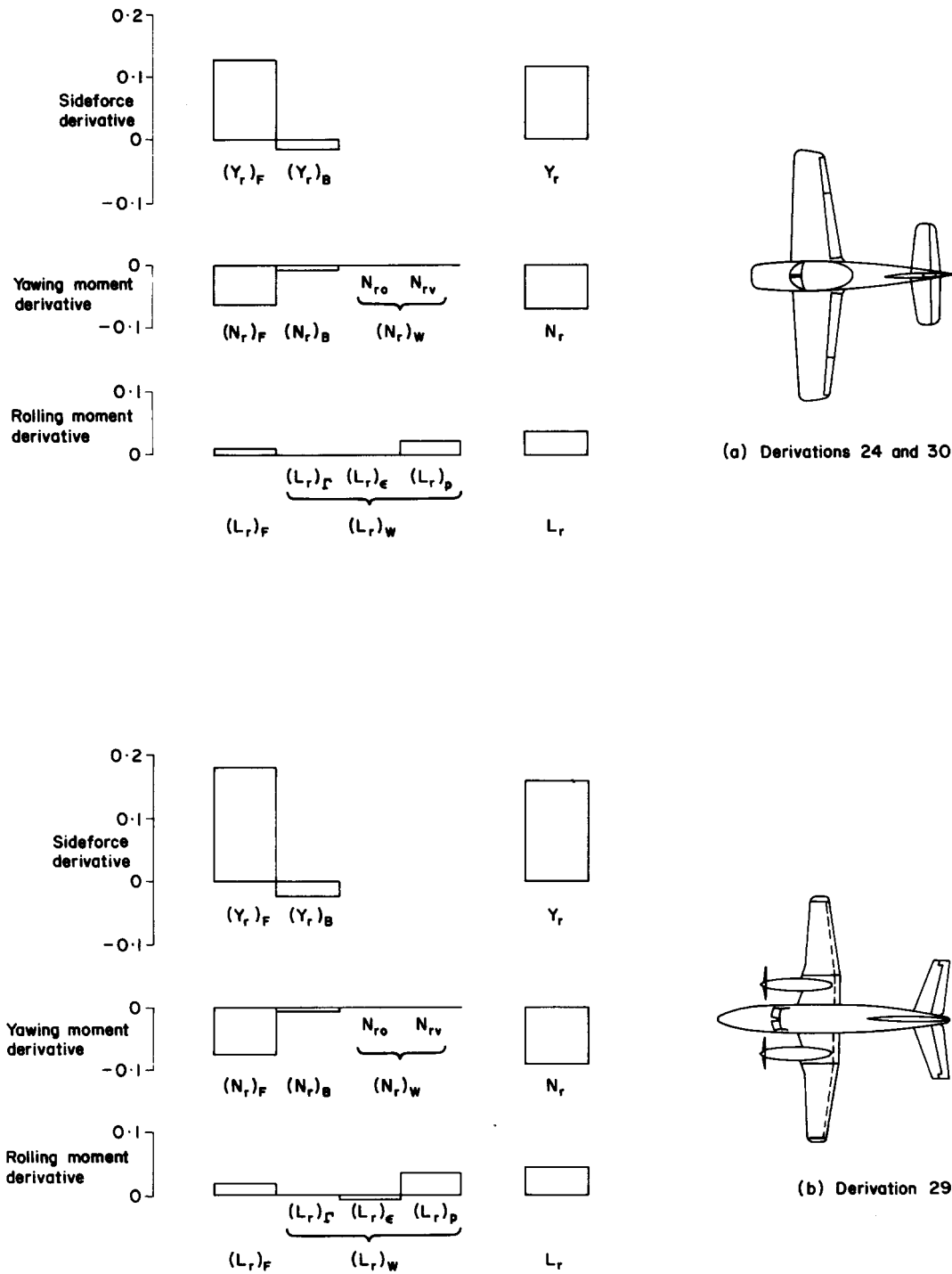—·—·— Landing configuration

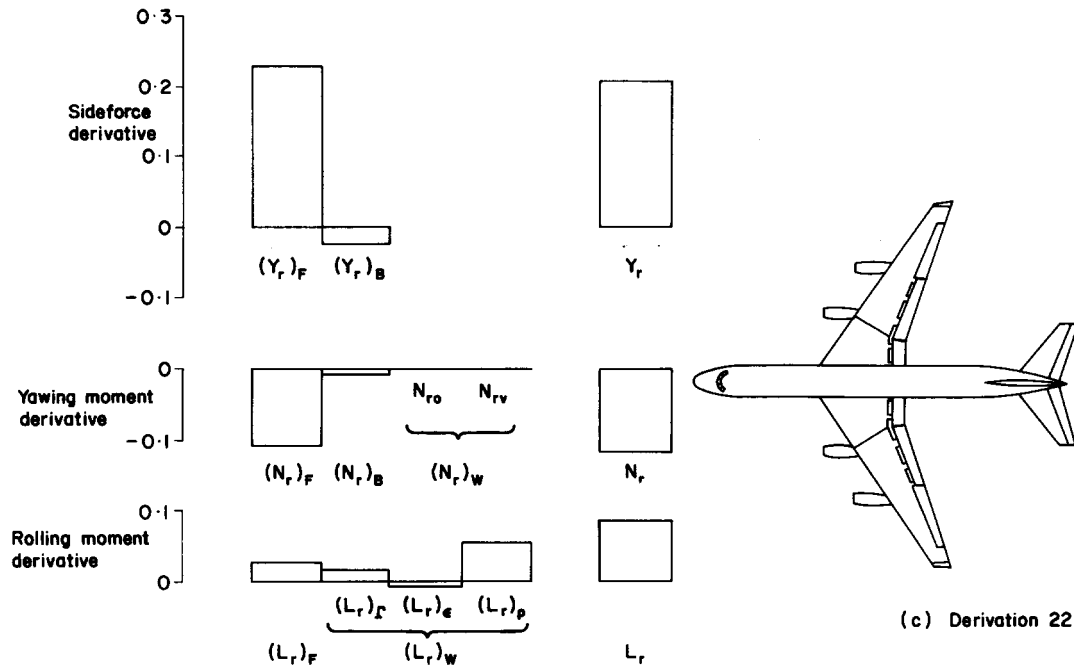**Sketch 3.5   Illustration of predicted and experimental values of Y_r and N_r**
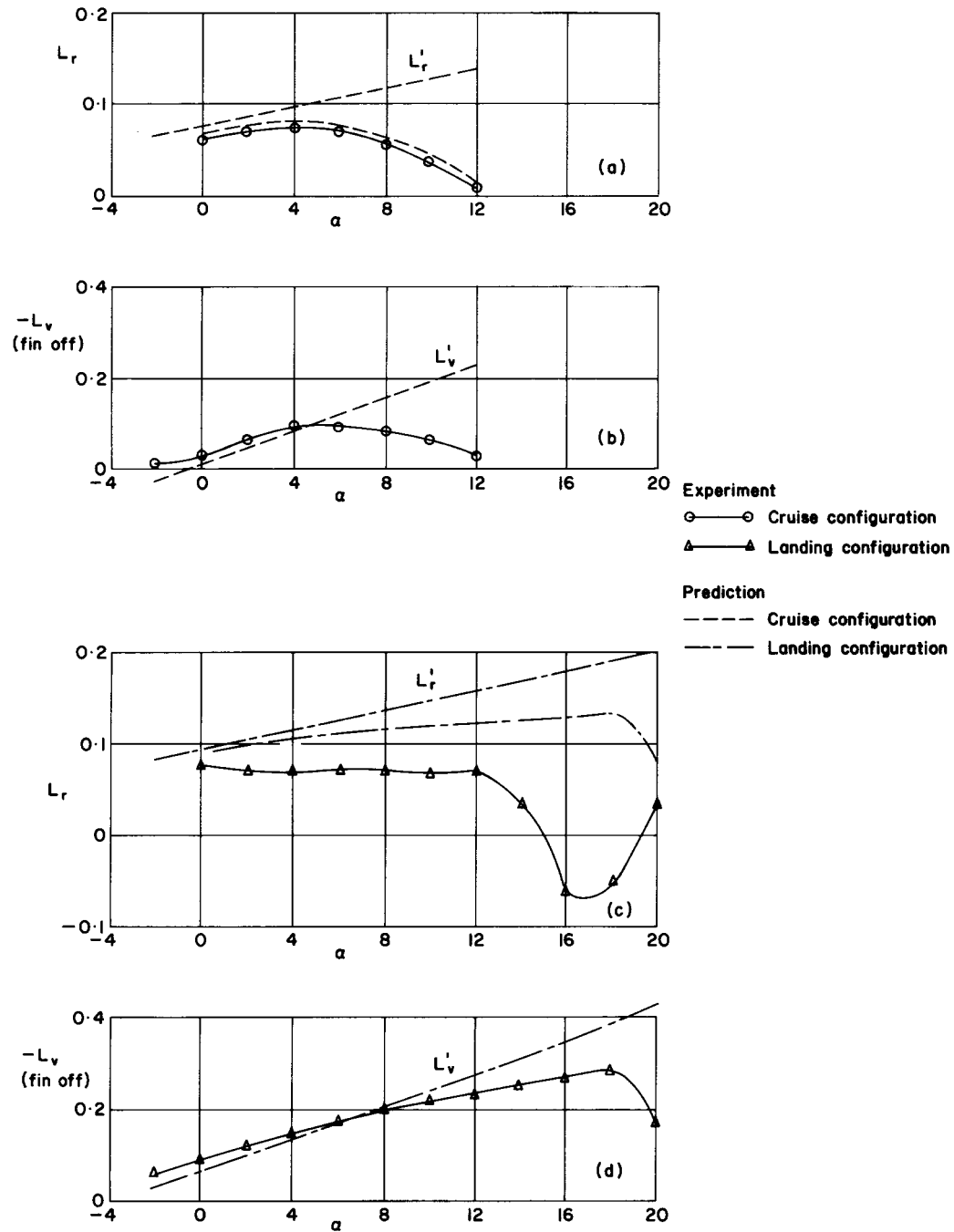
Sketch 3.6   Illustration of predicted and experimental values of L_r
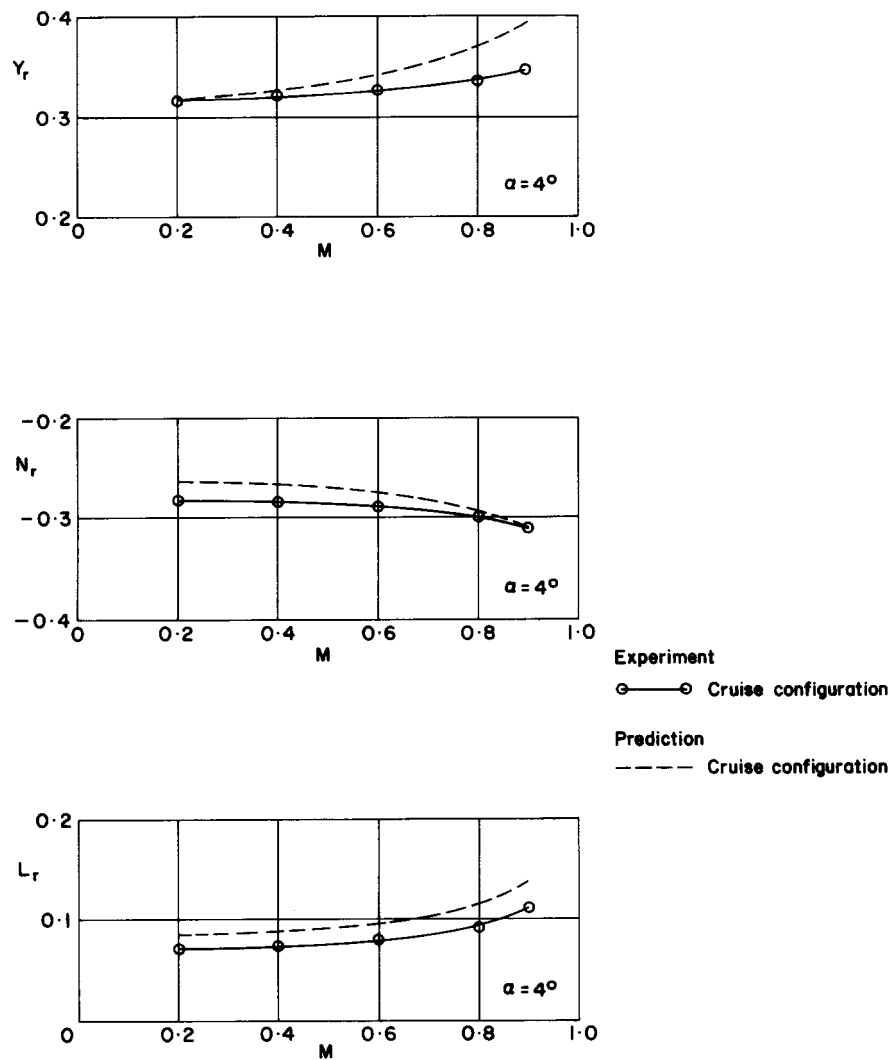
Sketch 3.7   Illustration of predicted and experimental variation with Mach number

(a) Derivations 24 and 30

(b) Derivation 29

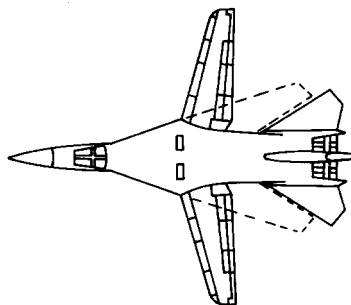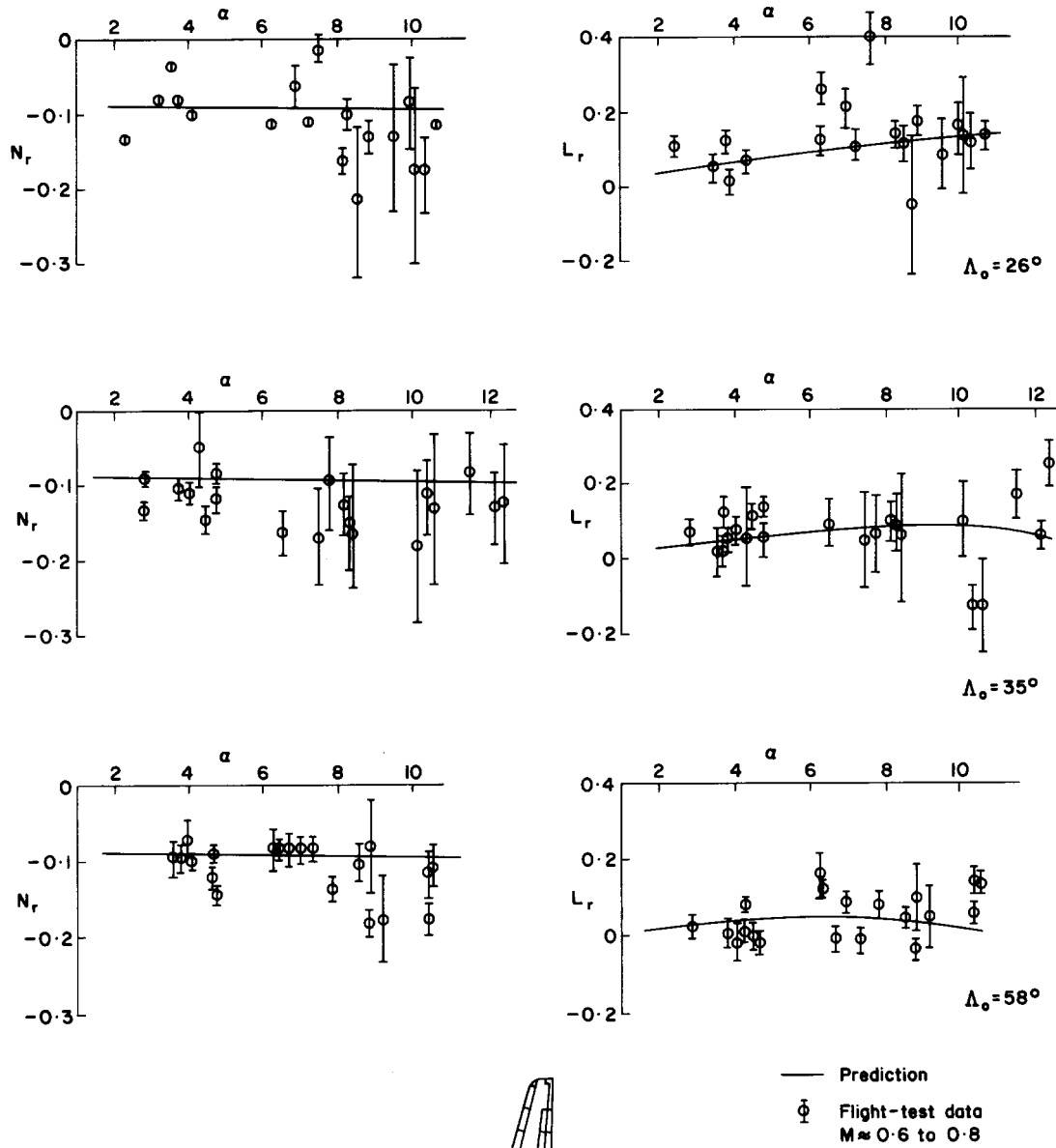**Sketch 3.8   Illustration of component break down for cruise conditions**

(c) Derivation 22
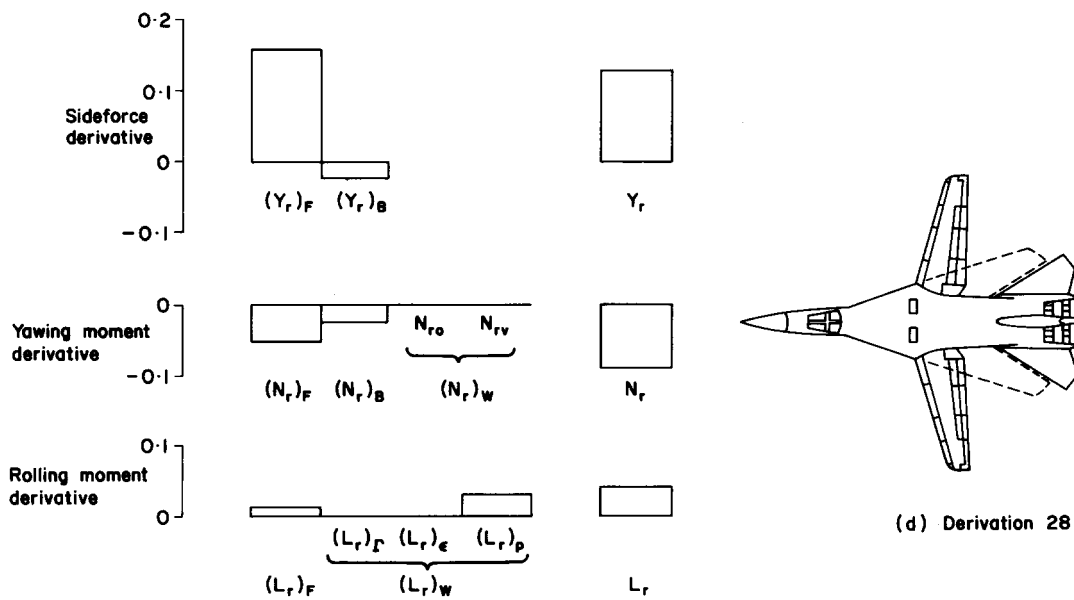
(d) Derivation 28

Sketch 3.8 (Concluded)

Sketch 3.9   Illustration of comparisons with flight-test data (Derivation 28)

4. DERIVATION AND REFERENCES

4.1 Derivation

The Derivation lists selected sources of information that have assisted in the preparation of this Item.

Wind-tunnel Data

1. BIRD, J.D.
JAQUET, B.M.
COWAN, J.W.
Effect of fuselage and tail surface on low-speed yawing characteristics of a swept-wing model as determined in curved-flow test section of Langley stability tunnel. NACA tech. Note 2483, 1948.

2. GOODMAN, A.
Effect of various outboard and central fins on low speed yawing stability derivatives of a 60° delta-wing model. NACA RM L50E12a (TIL 2411), 1950.

3. QUEIJO, M.J.
GOODMAN, A.
Calculations of the dynamic lateral stability characteristics of the Douglas D-588-II airplane in high-speed flight for various wing loadings and altitudes. NACA RM L50H16a (TIL 3352), 1950.

4. FISHER, L.R.
MICHAEL, W.H.
An investigation of the effect of vertical-fin location and area on low-speed lateral stability derivatives of a semitailess airplane model. NACA RM L51A10 (TIL 2655), 1951.

5. LETKO, W.
Effect of vertical-tail area and length on the yawing stability characteristics of a model having a 45° sweptback wing. NACA tech. Note 2358, 1951.

6. BIRD, J.D.
JAQUET, B.M.
Study of the use of experimental stability derivatives in the calculation of lateral disturbed motions of a swept-wing airplane and comparison with flight tests. NACA Rep. 1031, 1951.

7. QUEIJO, M.J.
WELLS, E.G.
Wind-tunnel investigation of the low-speed static and rotary stability derivatives of a 0.13-scale model of the Douglas D-558-II airplane in the landing configuration. NACA RM L52G07 (TIL 3502), 1952.

8. BIRD, J.D.
FISHER, L.R.
HUBBARD, S.M.
Some effects of frequency on the contribution of a vertical tail to the free aerodynamic damping of a model oscillating in yaw. NACA Rep. 1130, 1953.

9. FISHER, L.R.
FLETCHER, H.S.
Effect of lag of sidewash on the vertical-tail contribution to oscillatory damping in yaw of airplane models. NACA tech. Note 3356, 1954.

10. WILLIAMS, J.L.
Measured and estimated lateral static and rotary derivatives of a 1/12-scale model of a high-speed fighter airplane with unswept wings. NACA RM L53K09 (TIL 5187), 1954.

11. JAQUET, B.M.
FLETCHER, H.S.
Experimental steady-state yawing derivatives of a 60° delta-wing model as affected by changes in vertical position of the wing and in ratio of fuselage diameter to wing span. NACA tech. Note 3843, 1956.

12. BUELL, D.A.
REED, V.D.
LOPEZ, A.E.
The static and dynamic-rotary stability derivatives at subsonic speeds of an airplane model with an unswept wing and a high horizontal tail. NACA RM A56I04 (TIL 6655), 1956.

13. QUEIJO, M.J.
WELLS, E.G.
Effects of vertical fins near the nose of the fuselage on the directional and damping-in-yaw stability derivatives of an airplane model under steady-state and oscillatory conditions. NACA tech. Note 3814, 1956.

14. O'LEARY, C.O. — Transonic wind tunnel measurements of the oscillatory lateral aerodynamic derivatives of a BAC 221 model. RAE tech. Rep. 71098, 1971.

15. GRAFTON, S.B.
    LIBBEY, C.E. — Dynamic stability derivatives of a twin-jet fighter model for angles of attack from –10° to 110°. NASA tech. Note D-6091, 1971.

16. GRAFTON, S.B.
    CHAMBERS, J.R. — Wind-tunnel free-flight investigation of a model of a spin-resistant fighter configuration. NASA tech. Note D-7716, 1974.

17. COE, P.L.
    NEWSOM, W.A. — Wind-tunnel investigation to determine the low-speed yawing stability derivatives of a twin-jet fighter model at high angles of attack. NASA tech. Note D-7721, 1974.

18. O'LEARY, C.O. — Wind-tunnel measurement of lateral aerodynamic derivatives using a new oscillatory rig, with results and comparisons for the GNAT aircraft. ARC R&M 3847, 1977.

19. RAE — Unpublished wind-tunnel data from Royal Aircraft Establishment.

20. BAe — Unpublished wind-tunnel data from British Aerospace, Aircraft Group, Warton Division.

Flight-test data

21. HUNT, G.K. — Free flight model measurements of the dynamic stability of a supersonic strike aircraft. ARC CP 918, 1967.

22. TEPER, G.L. — Aircraft stability and control data. NASA CR 96008, 1969.

23. WOLOWICZ, C.H.
    YANCEY, R.B. — Lateral-directional aerodynamic characteristics of light twin-engine, propeller-driven airplanes. NASA tech. Note D-6946, 1972.

24. SUIT, W.T. — Aerodynamic parameters of the Navion airplane extracted from flight data. NASA tech. Note D-6643, 1972.

25. GILYARD, G.B. — Flight-determined derivatives and dynamic characteristics of the CV-990 airplane. NASA tech. Note D-6777, 1972.

26. SUIT, W.T.
    WILLIAMS, J.L. — Lateral static and dynamic aerodynamic parameters of the Kestrel aircraft (XV-6A) extracted from flight data. NASA tech. Note D-7455, 1974.

27. CANNADAY, R.L.
    SUIT, W.T. — Effects of control inputs on the estimation of stability and control parameters of a light aircraft. NASA tech. Paper 1043, 1977.

28. SIM, A.G.
    CURRY, R.E. — Flight-determined stability and control derivatives for the F-111 Tact research aircraft. NASA tech. Paper 1350, 1978.

29. TANNER, R.R.
    MONTGOMERY, T.D. — Stability and control derivative estimates obtained from flight data for the Beech 99 aircraft. NASA tech. Memo 72863, 1979.

30. SECKEL, E.
    MORRIS, J.J. — The stability derivatives of the Navion aircraft estimated by various methods and derived from flight test data. FAA-RD-71-6 (AD 723779), 1971.

ESDU Items

31. ESDU — Conversion factor for profile drag increment for part-span flaps. Item No. Aero F.02.01.07, ESDU International, June 1944.

32. ESDU — Profile drag coefficient increment due to full-span single slotted flaps (Handley Page and NACA types). Item No. Aero F.02.01.06, ESDU International, November 1944.

33. ESDU   Information on the use of Data Items on yawing moment derivatives of an aeroplane. Item No. Aero A.07.01.00, ESDU International, November 1946.

34. ESDU   Drag of a smooth flat plate at zero incidence. Item No. Aero W.02.04.01, ESDU International, July 1947.

35. ESDU   Profile drag of smooth wings. Item No. Aero W.02.04.02, ESDU International, July 1947.

36. ESDU   Lift coefficient increment due to full-span double flap (main flap slotted). Item No. Aero F.01.01.09, ESDU International, December 1948.

37. ESDU   Lift coefficient increment due to full-span slotted flaps. Item No. Aero F.01.01.08, ESDU International, March 1949.

38. ESDU   Profile drag of smooth aerofoils with straight trailing-edges at low speeds. Item No. Aero W.02.04.03, ESDU International, April 1953.

39. ESDU   Lift-curve slope of swept and tapered wings. Item No. Aero W.01.01.01, ESDU International, March 1953.

40. ESDU   Lift-curve slope for single fin and rudder. (i) Body shape merging into fin. Item No. Aero C.01.01.01, ESDU International, January 1955.

41. ESDU   Stability derivative $(L_v)_\Gamma$. Contribution of full-span dihedral to rolling moment due to sideslip. Item No. Aero A.06.01.03, ESDU International, April 1955.

42. ESDU   Stability derivative $(L_v)_\Gamma$. Contribution of part-span dihedral to rolling moment due to sideslip. Item No. Aero A.06.01.09, ESDU International, April 1955.

43. ESDU   Rate of change of lift coefficient with control deflection in incompressible two-dimensional flow, $(a_2)_0$. Item No. Aero C.01.01.03, ESDU International, May 1956.

44. ESDU   Information on the use of Data Items on rolling moment derivatives of an aeroplane. Item No. Aero A.06.01.00, ESDU International, March 1958.

45. ESDU   Lift-curve slope and aerodynamic centre position of wings in inviscid subsonic flow. Item No. 70011, ESDU International, July 1970.

46. ESDU   Aeronormalised stability derivatives: effect of wing on yawing moment due to yawing. Item No. 71017, ESDU International, September 1971.

47. ESDU   Effect of wing on rolling moment due to yawing. Item No. 72021, ESDU International, September 1972.

48. ESDU   Effects of isolated body and wing-body interference on rolling moment due to sideslip. Item No. 73006, ESDU International, June 1973.

49. ESDU   Lift coefficient increment at low speeds due to full-span split flaps. Item No. 74009, ESDU International, May 1974.

50. ESDU   Low-speed drag coefficient increment at zero lift due to full-span flaps. Item No. 74010, ESDU International, July 1974.

51. ESDU   Rate of change of lift coefficient with control deflection for full-span plain controls. Item No. 74011, ESDU International, July 1974.

52.	ESDU	Conversion of lift coefficient increment due to flaps from full span to part span. Item No. 74012, ESDU International, July 1974.
53.	ESDU	Information on the use of Data Items on flaps including estimation of the effects of fuselage interference. Item No. 75013, ESDU International, July 1975. (Superseded by Item Nos 97002 and 97003.)
54.	ESDU	Geometric properties of cranked and straight-tapered wing planforms. Item No. 76003, ESDU International, January 1976.
55.	ESDU	Contribution of wing planform to rolling moment derivative due to sideslip, $(L_v)_W$, at subsonic speeds. Item No. 80033, ESDU International, November 1980.
56.	ESDU	Effect of trailing-edge flaps on rolling moment derivative due to sideslip, $(L_v)_f$. Item No. 80034, ESDU International, November, 1980.
57.	ESDU	Estimation of rolling moment derivative due to sideslip for complete aircraft at subsonic speeds. Item No. 81032, ESDU International, October 1981.
58.	ESDU	Contribution of fin to sideforce, yawing moment and rolling moment derivatives due to sideslip, $(Y_v)_F$, $(N_v)_F$, $(L_v)_F$, in the presence of body, wing and tailplane. Item No. 82010, ESDU International, April 1982.
59.	ESDU	Estimation of sideforce and yawing moment derivatives due to sideslip for complete aircraft at subsonic speeds. Item No. 82011, ESDU International, September 1982.
60.	ESDU	Contribution of fin to sideforce, yawing moment and rolling moment derivatives due to rate of yaw $(Y_r)_F$, $(N_r)_F$, $(L_r)_F$. Item No. 82017, ESDU International, June 1982.
61.	ESDU	Contribution of body to yawing moment and sideforce derivatives due to rate of yaw, $(N_r)_B$ and $(Y_r)_B$. Item No. 83026, ESDU International, August 1983.

4.2   References

The References list selected sources of information supplementary to that given in this Item.

Rate of Change of Sideslip Derivatives

62.	COE, P.L. GRAHAM, A.B. CHAMBERS, J.R.	Summary of information on low-speed lateral-directional derivatives due to rate of change of sideslip β. NASA tech. Note D-7972, 1975.
63.	NGUYEN, L.T.	Evaluation of importance of lateral acceleration derivatives in extraction of lateral directional derivatives at high angles of attack. NASA tech. Note D-7739, 1974.

Correction to $(L_r)_W$

64.	CAMPBELL, J.P. GOODMAN, A.	A semi-empirical method for estimating the rolling moment due to yawing of airplanes. NACA tech. Note 1984, 1949.

Additional Flap Data

65.   YOUNG, A.D.   The aerodynamic characteristics of flaps. ARC R&M 2622, 1953.

Added since issue of Item No. 84002

66.   ESDU   Low-speed drag coefficient increment at constant lift due to full span plain flap. ESDU International, Item No. 87024, 1987.

67.   ESDU   Estimation of sideforce, yawing moment and rolling moment derivatives due to rate of roll for complete aircraft at subsonic speeds. ESDU Interantional, Item No. 85010, 1985

5. EXAMPLE

This Section provides a worked example to show how Y_r, N_r and L_r are calculated for the aircraft dimensioned as shown in Sketches 5.1 and 5.2 together with the additional geometric information in Table 5.1. Both inner and outer flaps are of the single-slotted type. The longitudinal body axis is taken parallel to the mid-body centre-line and passes through the aircraft centre of gravity position. Angles of attack are expressed in terms of this axis.

Calculations are performed for two flight conditions

(i)   a cruise condition with $\alpha = 0$, Mach number $= 0.78$ and Reynolds number/metre $= 7.5 \times 10^6$,

and

(ii)   a landing condition with $\alpha = 6°$, Mach number $= 0.20$ and Reynolds number/metre $= 4.5 \times 10^6$.

Where appropriate the components of Y_r, N_r and L_r are also expressed as functions of α. The variations of the total values are illustrated by sketches in Section 5.7.

It may be noted that the aircraft used in this example is the same as that in Item No. 81032 (Derivation 57) which demonstrates the calculation of L_v, and in Item No. 82011 (Derivation 59) which demonstrates the calculation of Y_v and N_v. Item No. 85010 (Derivation 67) illustrates the calculation of roll rate derivatives.

TABLE 5.1 Additional Geometric Parameters for Aircraft in Sketch 5.1

WING Angle between wing zero-lift line and longitudinal body axis Average section trailing-edge angle Average section thickness-to-chord ratio	3° 10° 0.10	
FLAPS (single slotted) Flap-chord to wing-chord ratio Flap-chord to extended-wing-chord ratio Extended-wing-chord to wing-chord ratio Flap deflection angle	At section FF' 0.250 0.238 1.05 45°	At section GG' 0.250 0.227 1.10 40°
BODY Maximum cross-sectional area Area of side elevation	28.3 m^2 224 m^2	
FIN Side area between tip and root chords	37.8 m^2	
Note (i) The wing and flap section parameters are taken in planes parallel to the aircraft plane of symmetry. (ii) Boundary-layer transition is assumed to occur at the leading edge of the wing.		
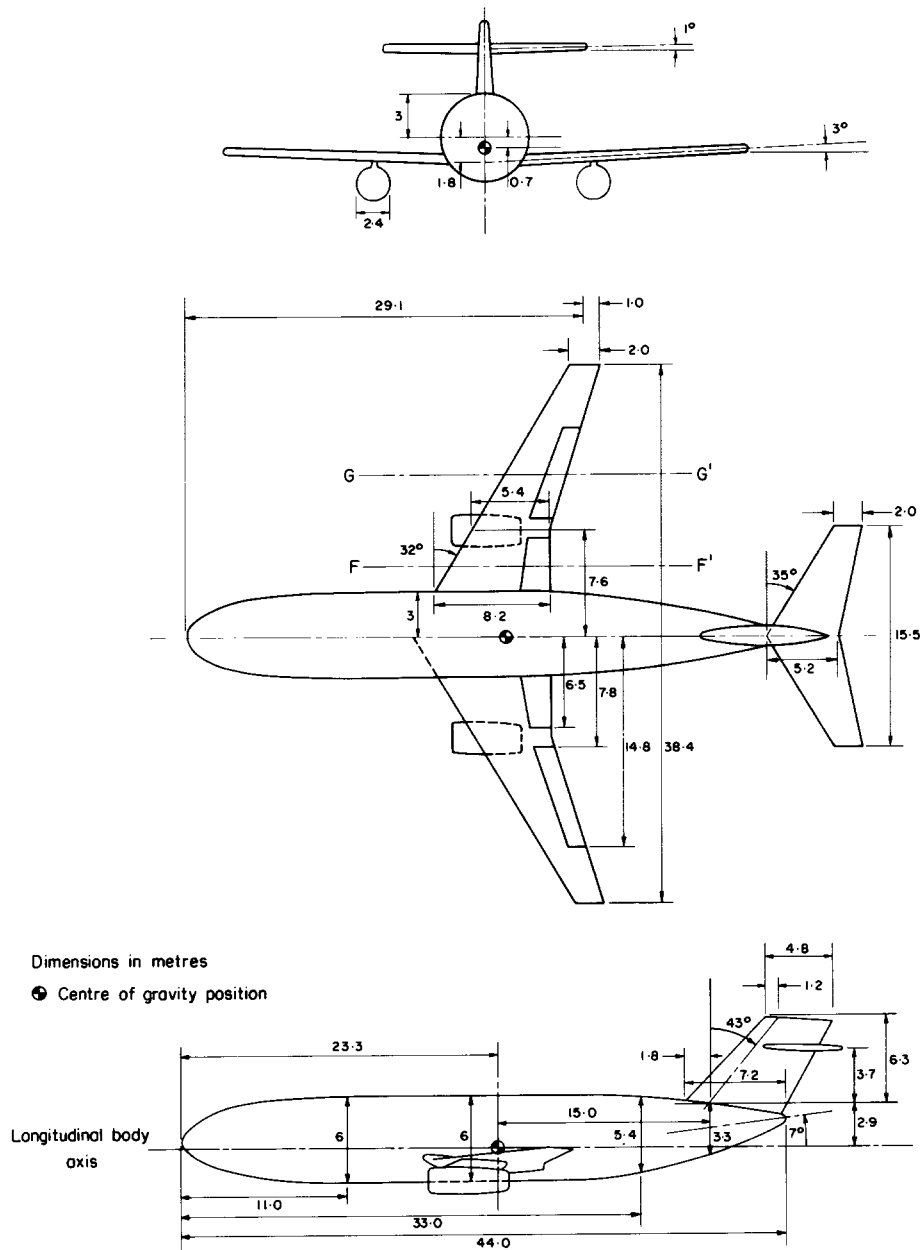
Sketch 5.1   Aircraft geometry
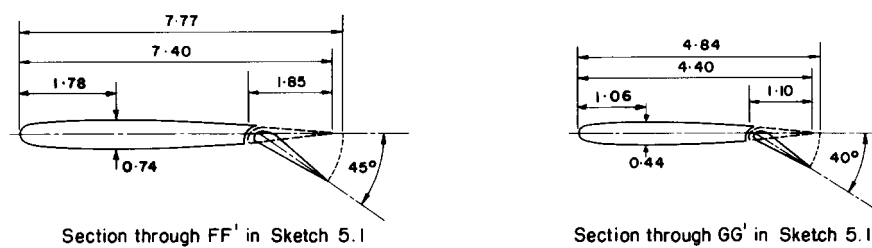
Sketch 5.2   Section geometry of flaps

5.1 Calculation of Wing Planform Parameters

See Item No. 76003 for Notation

Before commencing the estimation of Y_r, N_r and L_r it is usually necessary to calculate a number of geometric parameters for the wing planform that are not immediately available from Sketches 5.1, 5.2 or Table 5.1. This is because the Items dealing with the wing are only directly applicable to straight-tapered wings. Therefore, unless the aircraft has this type of wing, for which the planform parameters can be readily obtained from a scale diagram, a straight-tapered wing equivalent to the true wing has to be constructed by the method in the Addendum to Item No. 76003 (Derivation 54). That Item represents a cranked wing by a straight-tapered wing that has the same span, the same tip chord, and the same exposed wing area outside the intersection of the wing and body planforms, as the true wing. The equivalent-wing planform parameters that result from applying the method in Item No. 76003 to the aircraft in Sketch 5.1 are summarised in Table 5.2.

The values and notation in Table 5.2 are used throughout the example for the wing geometry.

TABLE 5.2 Properties of Equivalent Straight-tapered Wing Planform

Parameter	*Value*	*Parameter*	*Value*
Wing planform area, S	194.3 m^2	Leading-edge sweep, Λ_0	32.0°
Aspect ratio, A	7.59	Quarter-chord sweep, $\Lambda_{1/4}$	28.6°
Aerodynamic mean chord, $\bar{\bar{c}}$	5.68 m	Half-chord sweep, $\Lambda_{1/2}$	25.0°
Ratio of tip chord to root chord, λ	0.246		

5.2 Calculation of Wing and Flap Lift and Zero-lift Profile Drag Coefficients

Several of the yaw rate derivative components depend on the wing and flap lift and profile drag coefficients. The estimation of the necessary coefficients is described in Sections 5.2.1 and 5.2.2.

5.2.1 Wing Coefficients C_L, C_{D0}

The wing lift coefficient, C_L, may be estimated by using Item No. 70011 (Derivation 45) to obtain the lift-curve slope (per radian) that is appropriate to the equivalent wing values of $A \tan \Lambda_{\frac{1}{2}}$, $A(1-M^2)^{\frac{1}{2}}$ and λ. This is converted to the lift-curve slope per degree and multiplied by the angle of attack of the wing, $\alpha + \alpha_w$, where $\alpha_w = 3°$. For the wing parameters given in Table 5.2, $\partial C_L / \partial \alpha = 4.48/57.3$ per degree at $M = 0.2$ and $\partial C_L / \partial \alpha = 5.69/57.3$ per degree at $M = 0.78$. See Table 5.3 for a summary of results.

The profile drag coefficient of the wing, C_{D0}, may be estimated by using Item No. Aero W.02.04.01 (Derivation 34) to obtain a flat-plate skin friction coefficient at the Reynolds number of interest and then multiplying this by a wing profile ("lambda") correction factor taken from Item Nos Aero W.02.04.02 or 03 (Derivations 35 or 38). The correction factor depends on the position of maximum thickness, the thickness/chord ratio, the trailing-edge angle and the boundary-layer transition point of the wing section. For the wing section properties given in Sketch 5.2 and Table 5.1, $C_{D0} = 0.0062$ for a Reynolds number of 4.26×10^7 and $C_{D0} = 0.0067$ for a Reynolds number of 2.56×10^7, where the Reynolds numbers for $M = 0.78$ and 0.20 respectively are based on the aerodynamic mean chord of the equivalent wing $\bar{\bar{c}} = 5.68 \text{ m}$. See Table 5.4 for a summary of results.

TABLE 5.3 Wing Lift Coefficient

Parameter	Cruise Condition	Landing Condition (flaps retracted)
α	0	6°
M	0.78	0.20
$A(1-M^2)^{\frac{1}{2}}$	4.75	7.44
$A\tan\Lambda_{\frac{1}{2}}$	3.54	3.54
λ	0.246	0.246
$\partial C_L/\partial\alpha$ (per degree)	5.69/57.3	4.48/57.3
$\alpha + \alpha_w$	3°	9°
C_L	0.298	0.704[*]
C_L (as a function of α)	$0.0993(\alpha+3)$	$0.0782(\alpha+3)$[*]

[*]   Note this does not include the flap lift increment, see Section 5.2.3.

TABLE 5.4 Wing Zero-lift Profile Drag Coefficient

Parameter	Cruise Condition	Landing Condition (flaps retracted)
α	0	6°
M	0.78	0.20
Reynolds number based on $\bar{\bar{c}}$	4.26×10^7	2.56×10^7
Transition point	leading-edge	leading-edge
C_{D0} flat plate	0.00475	0.00515
Thickness chord ratio t/c	0.10	0.10
Maximum thickness	$0.24c$	$0.24c$
Trailing edge angle τ	10°	10°
Profile drag correction factor ("lambda")	1.30	1.30
C_{D0} wing	0.0062	0.0067[*]

[*]   Note this does not include the flap profile drag increment.

5.2.2 Flap Coefficients ΔC_{Lf}, ΔC_{D0f}.

For the single-slotted flaps that are shown in Sketches 5.1 and 5.2 Item No. Aero F.01.01.08 (Derivation 37) can be used to determine, separately, the full-span value of lift coefficient increment appropriate to the flap deflection and flap-chord to wing-chord ratios of the inner and outer panels. The part-span correction method in Item No. 74012 (Derivation 52) is then applied to reduce the full-span coefficients to the values appropriate to the spanwise extent of each panel. Note that the inner panel has a fictitious inboard extension added to account theoretically for body interference, as described in Item No. 75013 (Derivation 53). For an angle of attack of $\alpha = 6°$ those procedures give a lift coefficient of 0.369 for the inner panel and 0.356 for the outer panel, giving a total increment $\Delta C_{Lf} = 0.725$. The flap system considered in the example extends the local wing chord and therefore ΔC_{Lf} varies with α, but this variation is only about 10 per cent as α varies between 0 and 10° and for the purposes of the present example ΔC_{Lf} has been assumed to remain constant at its value for $\alpha = 6°$.

Similarly, Item No. Aero F.02.01.06 (Derivation 32) provides the full-span values of the profile drag coefficient increments, at zero lift, that are appropriate to the inner and outer flap panels, with the part-span correction method in Item No. Aero F.02.01.07 (Derivation 31) being used to allow for the spanwise extent of each panel. There is no body interference in this case. These procedures give a zero-lift profile drag coefficient of 0.014 for both the inner and outer panels and a total increment $\Delta C_{D0f} = 0.028$.

The flap coefficient increments are summarised in Table 5.5.

TABLE 5.5 Flap Lift and Zero-lift Profile Drag Coefficient Increments

Parameter	Landing Configuration (flaps deployed)		
	Inner flap panels	Outer flap panels	Total
ΔC_{Lf}	0.369	0.356	0.725
ΔC_{D0f}	0.014	0.014	0.028

The total lift coefficient of the wing at $M = 0.20$ with flaps deployed is therefore $C_L = 0.0782(\alpha + 3) + 0.725$. At $\alpha = 6°$ this gives $C_L = 0.704 + 0.725 = 1.429$.

5.2.3 Total Lift Coefficient

It is sometimes desirable to plot the stability derivatives against total C_L rather than angle of attack. In the present example, sufficiently accurate values of C_L are obtained for this by using values for the wing alone and for the wing with flaps deployed. No contribution is estimated for the tailplane since this is relatively small compared to the wing value; the minor contributions from the body and nacelles are also neglected. For other aircraft configurations, where the tail surface is large compared to the wing or where the body or nacelles provide a substantial part of the lift, their contributions should be included where possible.

The total lift for the cruise configuration is thus approximated by

$$C_L = (5.69/57.3)(\alpha + \alpha_w) = 0.0993(\alpha + 3) \,, \tag{5.1}$$

and for the landing configuration by

$$C_L = (4.48/57.3)(\alpha + \alpha_w) + \Delta C_{Lf} = 0.0782(\alpha + 3) + 0.725 \,. \tag{5.2}$$

5.3 Calculation of Wing and Flap Contributions* $(N_r)_W$ and $(N_r)_f$

See Item No. 71017 for Notation

5.3.1 Wing Yawing Moment Contribution

The value of $(N_r)_W$ is estimated using Item No. 71017, in which the derivative is divided into two components N_{r0} and N_{rv}, that are associated, respectively, with the asymmetric distributions of the wing profile drag, and the lift-dependent drag due to the trailing vortex system, that arise in yawing motion. The total contribution of the wing in terms of the wing profile drag coefficient C_{D0} and the wing lift coefficient C_L is

$$(N_r)_W = \left(\frac{N_{r0}}{C_{D0}}\right)C_{D0} + \left(\frac{N_{rv}}{C_L^2}\right)C_L^2 \ . \tag{5.3}$$

Item No. 71017 gives a carpet for $(N_{r0}/C_{D0})_{\lambda = 1}$, as a function of A and $\Lambda_{1/4}$ for the taper ratio $\lambda = 1$. A factor $(N_{r0}/C_{D0})_\lambda/(N_{r0}/C_{D0})_{\lambda = 1}$ is given as a function of λ for correcting to other taper ratios.

The parameter N_{rv}/C_L^2 is given as a series of carpets in terms of A and $\Lambda_{1/4}$ at $\lambda = 0$, 0.25, 0.5 and 1.

Item No. 71017 recommends that the effects of compressibility on $(N_r)_W$ can be largely accounted for by use of the C_L and C_{D0} values appropriate to the required Mach number and by replacing A and $\Lambda_{1/4}$ in the carpets by $A(1 - M^2)^{1/2}$ and $\tan^{-1}[(1 - M^2)^{-1/2}\tan\Lambda_{1/4}]$, respectively. See Table 5.6 for a summary of the results, C_L and C_{D0} being obtained from Section 5.2.

5.3.2 Flap Yawing Moment Contribution

Item No. 71017 estimates the contribution caused by trailing-edge flap deployment by considering the changes that this produces in the lift and profile drag coefficients. The effect of the change in lift coefficient is allowed for by simply multiplying the wing-alone value of N_{rv}/C_L^2 by the value of C_L^2 appropriate to the wing with flaps deployed. This part of the flap effect is therefore automatically included in $(N_r)_W$ once the correct value of lift coefficient is used.

The effect of the profile drag coefficient is estimated through the formula

$$\Delta N_{r0} = \left(\frac{N_{r0}}{C_{D0}}\right) f \sec^2(\Lambda_{1/4})\Delta C_{D0f}, \tag{5.4}$$

where N_{r0}/C_{D0} is the wing-alone value and f is a function of flap span, b_f/b, and wing taper ratio, λ. Equation (5.4) represents the flap contribution at constant C_L. In the notation of this Item this is written $(N_r)_f$, and is exactly equivalent to the ΔN_{r0} term in Item No. 71017.

Item No. 71017 deals only with a single trailing-edge flap on each wing and does not describe how to cope with inner and outer panels. However, the method for predicting the flap contribution is tentative, since it is based on a small number of data, and the flap contribution $(N_r)_f$ ($\equiv \Delta N_{r0}$) is a small quantity. Therefore it is suggested that the outer limit of the outer panel be used to define b_f/b, with the total increment in profile drag coefficient from both inner and outer panels being substituted for ΔC_{D0f} in Equation (5.4). See Table 5.6 for a summary of the results; C_L, C_{D0}, ΔC_{Lf} and ΔC_{D0f} being obtained from Section 5.2.

---

* The wing and flaps are assumed to have a negligible effect on Y_r.

TABLE 5.6 Calculation of $(N_r)_W$ and $(N_r)_f$

Parameter	Cruise Configuration	Landing Configuration
α	0	6°
M	0.78	0.20
C_L (flaps retracted)	0.298	0.704
C_L (flaps deployed)	–	1.429
A	7.59	7.59
$\Lambda_{1/4}$	28.6°	28.6°
$A(1-M^2)^{1/2}$	4.75	7.44
$\tan^{-1}[(1-M^2)^{-1/2}\tan\Lambda_{1/4}]$	41.1°	29.1°
$(N_{r0}/C_{D0})_{\lambda=1}$	–0.243	–0.200
λ	0.246	0.246
$\left[\dfrac{(N_{r0}/C_{D0})_{\lambda}}{(N_{r0}/C_{D0})_{\lambda=1}}\right]$	0.70	0.70
N_{r0}/C_{D0}	–0.170	–0.140
C_{D0} (flaps retracted)	0.0062	0.0067
ΔC_{D0f}	–	0.028
b_f/b	–	0.770
f	–	0.595
N_{r0}	–0.0011	–0.00094
N_{rv}/C_L^2	–0.0065	–0.0050
N_{rv}	–0.00058	–0.0102
$(N_r)_W = N_{r0} + N_{rv}$	–0.0017	–0.0111
$(N_r)_W$ as a function of α	$\begin{cases} -0.0011 \\ -0.000641(\alpha+3)^2 \end{cases}$	$\begin{cases} -0.00094 \\ -0.005\,(0.0782(\alpha+3)+0.725)^2 \end{cases}$
$(N_r)_f\ (\equiv \Delta N_{r0})$	–	–0.0030

As pointed out in the text the $(N_r)_W$ derivative for the landing configuration that is given in Table 5.6 includes the contribution due to the lift coefficient increment associated with the deployment of trailing-edge flaps. This forms a significant part of $(N_r)_W$. For example, at $\alpha = 6°$ and $M = 0.2$ the clean wing value of $(N_r)_W$ is –0.0025 so at this flight condition the flap lift coefficient increment contributes –0.0086 towards the landing-configuration value of –0.0111, and this contribution is about three times the value of $(N_r)_f$. It should, however, be noted that for most configurations $(N_r)_W$ and $(N_r)_f$ are very small compared to the fin contribution $(N_r)_F$, see Section 5.7.

5.4 Calculation of Wing and Flap Contributions $(L_r)_W$ and $(L_r)_f$

See Item No. 72021 for Notation

5.4.1 Wing Rolling Moment Contribution

The attached flow value $(L'_r)_W$ is estimated using Item No. 72021. This derivative arises from the lift differential between the wing panels that occurs in yawing motion. For calculation purposes it is divided into three components, $(L_r)_p$, $(L_r)_\Gamma$ and $(L_r)_\varepsilon$, that are associated, respectively, with the wing planform in attached flow, the wing dihedral, and the wing twist. See also Section 5.4.3 where a correction is made for the effects of flow separation.

The planform component in attached flow is proportional to the wing lift coefficient and Item No. 72021 gives a carpet for $(L_{r0})_p / g(\Lambda_{1/4}) C_L$ in terms of A and λ where $(L_{r0})_p$ is the incompressible flow value of $(L_r)_p$ and $g(\Lambda_{1/4})$ is a factor, given as a function of $\Lambda_{1/4}$, that allows for the wing sweep. (Separate data are presented for slender delta and gothic wings with aspect ratios less than unity.)

The incompressible flow value of the dihedral component is given in terms of the parameter $(L_{r0})_\Gamma / \Gamma$, which is a function of $\Lambda_{1/4}$ only.

The incompressible flow value of the twist component is given in terms of the parameter $(L_{r0})_\varepsilon / \varepsilon$, which is plotted as a carpet in terms of A and λ for $\Lambda_{1/4} = 0$. The factor $g(\Lambda_{1/4})$ is applied to account for different wing sweep angles. The data for $(L_{r0})_\varepsilon / \varepsilon$ apply only to uniform twist along the wing and are therefore limited in application but may be used to approximate the influence of wing twist.

To allow for compressibility effects Item No. 72021 contains a series of carpets giving the correction factor L_r / L_{r0} in terms of A and $\Lambda_{1/4}$ for $M = 0.4, 0.6, 0.7, 0.8$ and 0.9. Although derived for the planform component only, Item No. 72021 suggests that the factor be applied to the total value of L_r since $(L_r)_p$ is usually far more significant than $(L_r)_\Gamma$ or $(L_r)_\varepsilon$.

Table 5.7 summarises the results of the calculation of $(L_r)_W$, C_L being taken from Section 5.2.

5.4.2 Flap Rolling Moment Contribution

Item No. 72021 estimates the contribution caused by trailing-edge flap deployment by multiplying the clean-wing value of $(L_r)_p / C_L$ by the lift coefficient appropriate to the wing with flaps deflected, and adding a term, $(L_r)_f$, to provide the flap contribution at constant C_L. The flap effect associated with the increment in lift coefficient due to the flaps is thus automatically included in the derivative $(L_r)_p$ once the correct value of lift coefficient is used.

The incompressible flow value of $(L_r)_f$ is given, at $\Lambda_{1/4} = 0$, in terms of an aspect ratio factor $f_2(A)$ and the parameter $a_{2\infty} \delta_f / 2\pi$, that can be considered as the change in incidence at constant lift coefficient equivalent to the deflection of the flaps in two-dimensional flow. The term $a_{2\infty}$ (rad^{-1}) is the slope of the lift increment curve with flap deployment in two-dimensional flow and δ_f (deg) is the deflection angle of the flap main element. Item No. 72021 gives the function $f_2(A)$ plotted against A, and the parameter $(L_{r0})_f / [f_2(A) a_{2\infty} \delta_f / 2\pi]$ plotted against the flap inboard and outboard limits $(b_f / b)_{i/b}$ and $(b_f / b)_{0/b}$. The factor $g(\Lambda_{1/4})$ is used to allow for other wing sweep angles and, if necessary, the factor L_r / L_{r0} is used to allow for compressibility effects. For any particular flap system, values of $(L_r)_f$ are calculated from the curves at $(b_f / b)_{i/b}$ and $(b_f / b)_{0/b}$, and the difference between these values gives the value of $(L_r)_f$ appropriate to the flap system of interest.

As stated in Item No. 72021 the parameter $a_{2\infty}$ may be satisfactorily estimated for plain flaps by using the inviscid flow value of $a_{2\infty}$ given by Item No. Aero C.01.01.03 (Derivation 43). For split flaps a two-dimensional value of ΔC_{Lf} can be estimated from Item No. 74009 and set equal to $a_{2\infty}\delta_f/57.3$. For slotted flaps Item No. Aero F.01.01.08 or 09 may be used to calculate a value of ΔC_{Lf} at $A = 6$ which can be multiplied by 1.4 to obtain a two-dimensional value that can then be set equal to $a_{2\infty}\delta_f/57.3$.

Under the assumption that the flaps of the present example are each fitted as full-span flaps to an unswept, untapered wing of aspect ratio 6, Item No. Aero F.01.01.08 gives values of flap lift increment $\Delta C_{Lf} = 1.073$ for the inner flaps and $\Delta C_{Lf} = 1.089$ for the outer flaps. These are multiplied by 1.4 to convert them to two-dimensional values and set equal to $a_{2\infty}\delta_f/57.3$ to give

$$a_{2\infty}\delta_f/2\pi = 57.3 \times 1.4 \times 1.073/2\pi = 13.7° \text{ for the inner flaps}$$

and $\qquad a_{2\infty}\delta_f/2\pi = 57.3 \times 1.4 \times 1.089/2\pi = 13.9°$ for the outer flaps.

The remaining calculations for $(L_r)_f$ are summarised in Table 5.7.

As pointed out in the text, for the landing configuration the $(L_r)_p$ derivative and hence the $(L'_r)_W$ derivative that is given in Table 5.7 includes the contribution due to the lift coefficient increment associated with the deployment of trailing-edge flaps. This forms a significant part of $(L'_r)_W$. For example, at $\alpha = 6°$ and $M = 0.2$ the clean wing value of $(L'_r)_W$ is 0.1032 so at this flight condition the flap lift coefficient increment contributes 0.1092 towards the landing-configuration value of $(L'_r)_W = 0.2124$, and is very much larger than the value of $(L_r)_f$, see Section 5.7.

5.4.3 Calculation of $(\Delta L_r)_{corr}$

As explained in Section 3.3.2, partial flow separation causes experimental values of $(L_r)_W$ to depart rapidly from the values predicted for attached flow. A correction for this is made through Equations (3.2) and (3.3),

$$(\Delta L_r)_{corr} = 0.5[(L'_{v\ pred} - L'_{v0\ pred}) - (L_{v\ exp} - L_{v0\ exp})]$$

and $\qquad (L_r)_W = (L'_r)_W + (\Delta L_r)_{corr}.$

In Equation (3.2) the values of L_v may be for the isolated wing, the wing-body or the complete aircraft, provided that the same configuration is taken throughout. However, as discussed in the main text a more accurate result will generally be obtained by using data for the simpler configurations.
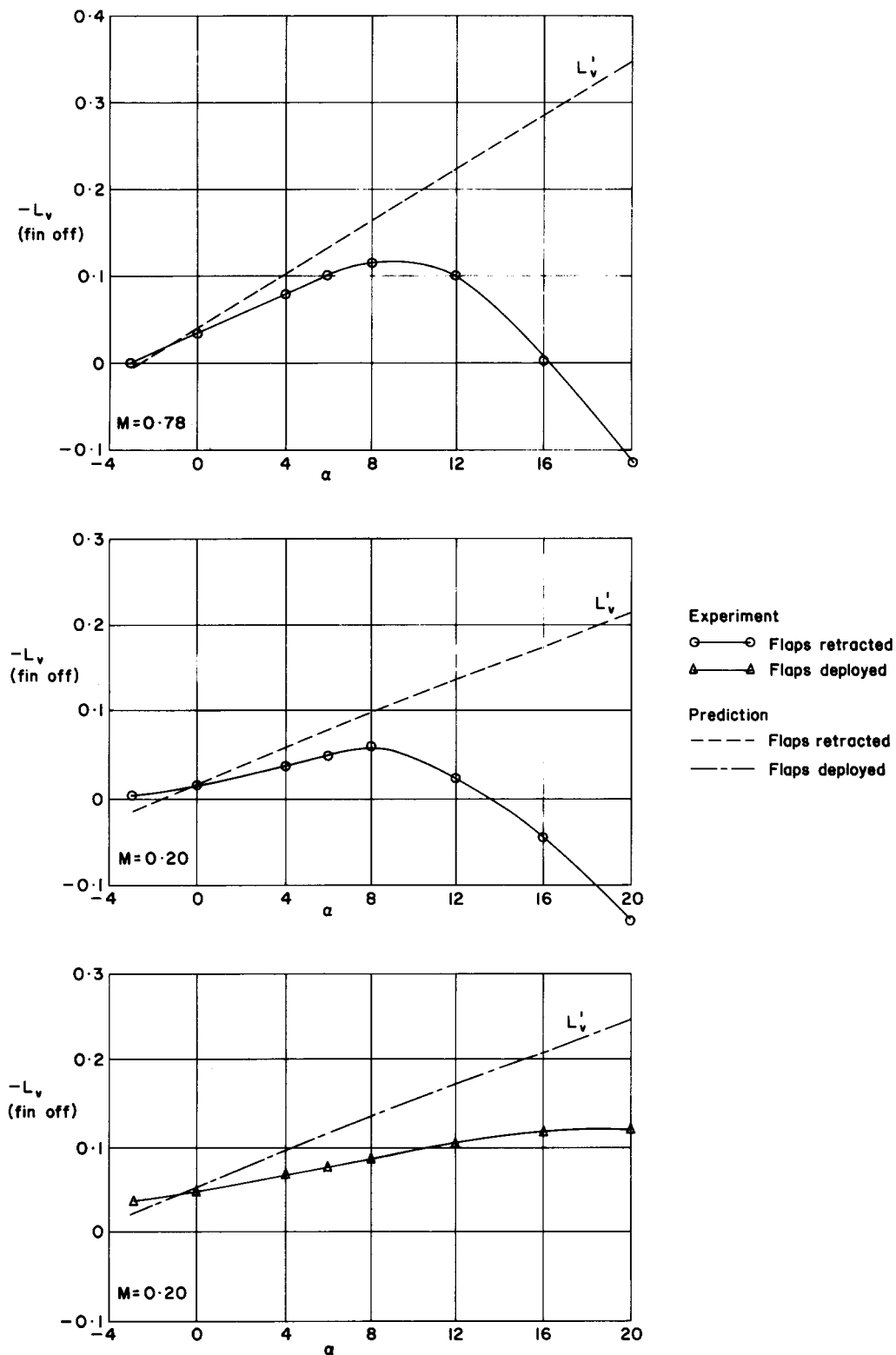
Sketch 5.3 shows assumed experimental values of L_v for the wing-body and wing-body-flap configurations of this example, together with their theoretical predictions that have been taken from Item No. 81032. Table 5.8 sets these results out numerically as a function of α and gives the values of $(\Delta L_r)_{corr}$ that are calculated from Equation (3.2) by using the wing-body or wing-body-flap values of L_v. The L_{v0} values corresponding to zero wing C_L are taken from the $\alpha = -3°(= -\alpha_W)$ column. Table 5.8 also shows the predicted values of $(L'_r)_W$ from Table 5.7 and the corrected values $(L_r)_W$ that result from Equation (3.3). Those derivatives are illustrated in Sketch 5.4.

TABLE 5.7 Calculation of $(L'_r)_W$ and $(L_r)_f$

Parameter	Cruise Configuration	Landing Configuration	
α	0	6°	
M	0.78	0.20	
A	7.59	7.59	
$\Lambda_{1/4}$	28.6°	28.6°	
λ	0.246	0.246	
Γ (dihedral angle)	3°	3°	
ε (twist angle)	3°	3°	
C_L (flaps retracted)	0.298	0.704	
C_L (flaps deployed)	–	1.429	
$(L_{r0})_p/g(\Lambda_{1/4})C_L$	0.1004	0.1004	
$g(\Lambda_{1/4})$	1.50	1.50	
$(L_{r0})_\Gamma/\Gamma$	0.00108 deg^{-1}	0.00108 deg^{-1}	
$(L_{r0})_\varepsilon/\varepsilon$	–0.0017 deg^{-1}	–0.0017 deg^{-1}	
(L_r/L_{r0})	1.35	1	
$(L_r)_p = \left[\dfrac{(L_{r0})_p}{g(\Lambda_{1/4})C_L}\right]g(\Lambda_{1/4})C_L\left(\dfrac{L_r}{L_{r0}}\right)$	0.0606	0.2152	
$(L_r)_p$ as a function of α	$0.0202(\alpha+3)$	$0.01178(\alpha+3)+0.1092$	
$(L_r)_\Gamma = \left[\dfrac{(L_{r0})_\Gamma}{\Gamma}\right]\Gamma\left(\dfrac{L_r}{L_{r0}}\right)$	0.0066	0.0049	
$(L_r)_\varepsilon = \left[\dfrac{(L_{r0})_\varepsilon}{\varepsilon}\right]_{\Lambda_{1/4}=0}\varepsilon\,g(\Lambda_{1/4})\left(\dfrac{L_r}{L_{r0}}\right)$	–0.0103	–0.0077	
$(L'_r)_W = (L_r)_p + (L_r)_\Gamma + (L_r)_\varepsilon$	0.0569	0.2124	
$(L'_r)_W$ as a function of α	$0.0202(\alpha+3)-0.0037$	$0.01178(\alpha+3)+0.1064$	
		inner flaps	outer flaps
$a_{2\infty}\delta_f/2\pi$	–	13.7°	13.9°
$(b_f/b)_{i/b}$	–	0.156	0.406
$(b_f/b)_{o/b}$	–	0.338	0.770
$((L_{r0})_f/[f_2(A)a_{2\infty}\delta_f/2\pi])_{i/b}$	–	–0.00145	–0.00325
$((L_{r0})_f/[f_2(A)a_{2\infty}\delta_f/2\pi])_{o/b}$	–	–0.00285	–0.00205
$f_2(A)$	–	0.84	
$(L_r)_f$	–	–0.0032*	

$$* \ (L_r)_f = \sum\left\{\left[\frac{(L_{r0})_f}{f_2(A)a_{2\infty}\delta_f/2\pi}\right]_{o/b} - \left[\frac{(L_{r0})_f}{f_2(A)a_{2\infty}\delta_f/2\pi}\right]_{i/b}\right\}[f_2(A)a_{2\infty}\delta_f/2\pi]g(\Lambda_{1/4})\left(\frac{L_r}{L_{r0}}\right).$$

The contributions of the inner and outer panels are –0.0242 and +0.0210 respectively.

Sketch 5.3   Predicted and experimental values of L_v
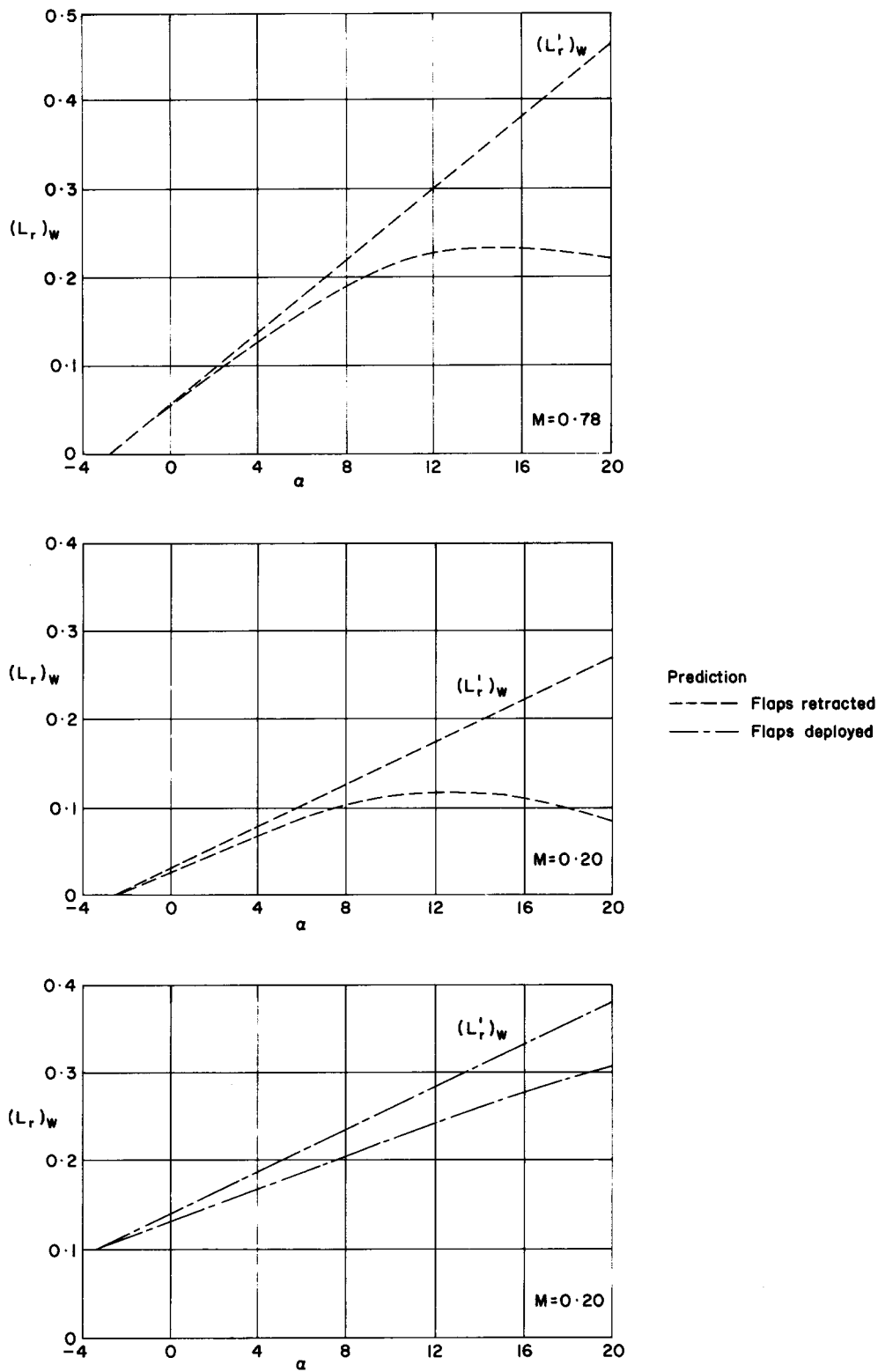
Sketch 5.4   Comparison of corrected and uncorrected values of $(L_r)_W$

TABLE 5.8 Application of correction $(\Delta L_r)_{corr}$

α (degrees)	–3	0	4	6	8	12	16	20	Condition
$L_{v\ exp}$	0.000	–0.036	–0.075	–0.100	–0.115	–0.100	0.000	–0.120	$M = 0.78$
$L'_{v\ pred}$	0.008	–0.039	–0.092	–0.131	–0.162	–0.224	–0.286	–0.348	Flaps
$(\Delta L_r)_{corr}$	0.000	–0.006	–0.013	–0.020	–0.028	–0.066	–0.147	–0.238	retracted.
$(L'_r)_W$	–0.004	0.057	0.138	0.178	0.219	0.299	0.380	0.461	Fin off.
$(L_r)_W$	–0.004	0.051	0.125	0.158	0.191	0.233	0.233	0.223	
$L_{v\ exp}$	0.000	–0.015	–0.040	–0.050	–0.060	–0.025	0.050	0.140	$M = 0.2$
$L'_{v\ pred}$	0.012	–0.018	–0.057	–0.076	–0.096	–0.134	–0.173	–0.212	Flaps
$(\Delta L_r)_{corr}$	0.000	–0.008	–0.015	–0.019	–0.024	–0.061	–0.118	–0.182	retracted.
$(L'_r)_W$	–0.003	0.033	0.080	0.103	0.127	0.174	0.221	0.268	Fin off.
$(L_r)_W$	–0.003	0.025	0.065	0.084	0.103	0.113	0.113	0.086	
$L_{v\ exp}$	–0.040	–0.050	–0.070	–0.078	–0.085	–0.105	–0.120	–0.120	$M = 0.2$
$L'_{v\ pred}$	–0.026	–0.056	–0.095	–0.114	–0.134	–0.176	–0.211	–0.250	Flaps
$(\Delta L_r)_{corr}$	0.000	–0.010	–0.020	–0.025	–0.032	–0.043	–0.053	–0.072	deployed.
$(L'_r)_W$	0.106	0.142	0.189	0.212	0.236	0.283	0.330	0.377	Fin off.
$(L_r)_W$	0.106	0.132	0.169	0.187	0.204	0.240	0.277	0.305	

The primes denote values for attached flow.

5.5 Calculation of Body Contributions $(Y_r)_B$ and $(N_r)_B$

See Item No. 83026 for Notation

The values of $(Y_r)_B$ and $(N_r)_B$ are evaluated using Item No. 83026. That Item uses slender-body theory to predict $(N_r)_B$ for bodies with finite base areas and an empirical correlation for bodies with zero base areas. The latter approach applies in the present example, and the required equation is

$$(N_r)_B b^2 S / l_b^2 S_b = -0.01 \ , \tag{5.5}$$

where l_b is the body length and S_b the side elevation area of the body. (Note that the wing reference area S is denoted by the symbol S_W in Item No. 83026; S has been used here to provide consistency with other sections.)

The value of $(Y_r)_B$ is obtained by a purely empirical method that is assumed to be applicable to all classes of body,

$$(Y_r)_B b S / l_b S_b = -0.04 \ . \tag{5.6}$$

Table 5.9 sets out the results of using Equations (5.5) and (5.6). The body provides a small contribution to N_r, acting in the same sense as the fin component (see Section 5.7). The body contribution to Y_r is fairly significant and opposes the fin component (see Section 5.7). Both derivatives are independent of angle of attack and Mach number.

TABLE 5.9 Calculation of $(Y_r)_B$ and $(N_r)_B$

Parameter	Cruise and Landing Configuration
b	38.4 m
S	194.3 m^2
l_b	44.0 m
S_b	224.0 m^2
$(N_r)_B b^2 S / l_b^2 S_b$	–0.01
$(N_r)_B$	–0.015
$(Y_r)_B b S / l_b S_b$	–0.04
$(Y_r)_B$	–0.053

5.6 Calculation of Fin Contributions $(Y_r)_F$, $(N_r)_F$ and $(L_r)_F$

See Item No. 82017 for Notation

The fin contributions are calculated by the method in Item No. 82017 which makes use of the lift-curve slope and the centre of pressure position of the fin sideforce in steady sideslip, together with an effective sideslip angle that is equal to the product of the yaw rate and the moment arm of the fin sideforce.

The fin contributions are given by the equations

$$(Y_r)_F = -\,[(Y_v)_F]_{J_W = 1}(\bar{l}'_F \cos\alpha \,+\, \bar{z}'_F \sin\alpha)/b\,, \tag{5.7}$$

$$(N_r)_F = -\,(Y_r)_F(\bar{l}'_F \cos\alpha \,+\, \bar{z}'_F \sin\alpha)/b \tag{5.8}$$

and

$$(L_r)_F = (Y_r)_F(\bar{z}'_F \cos\alpha \,-\, \bar{l}'_F \sin\alpha)/b\,, \tag{5.9}$$

where $[(Y_v)_F]_{J_W = 1}$ is the sideforce derivative due to sideslip for the fin in the presence of the body and tailplane, but with the subscript $J_W = 1$ denoting that no allowance is to be made for wing interference (see Item No. 82017). The lengths $\bar{z}'_F$ and $\bar{l}'_F$ are measured normal and parallel to the longitudinal body axis, respectively, and define the distance between the aircraft centre of gravity position and the centre of pressure position of the fin sideforce. For aircraft with fin-tailplane assemblies of the type considered in this example $[(Y_v)_F]_{J_W = 1}$ can be calculated from Item No. 82010. (The data in Item No. Aero C.01.01.01 can be used for aircraft where the rear body is very narrow and merges into the fin.)

The results of the calculation for $(Y_r)_F$, $(N_r)_F$ and $(L_r)_F$ are set out in Table 5.10. The fin contributions are usually very important and in the case of Y_r and N_r normally provide the dominant component, see Section 5.7.

Note that if wind-tunnel static lateral stability data are available for models of the aircraft of interest with and without a fin, then these may be used directly to determine the experimental values of the derivatives $(Y_v)_F$, $(N_v)_F$ and $(L_v)_F$. By comparing these values with those calculated from Item No. 82010 empirical corrections can be determined which may be used to increase or reduce the values of $[(Y_v)_F]_{J_W = 1}$, $\bar{l}'_F$ and $\bar{z}'_F$ to be employed in Equations (5.7) to (5.9). In particular, values of $(L_v)_F/(Y_v)_F$ from experiment may be used to determine the tail arm $(\bar{z}'_F \cos\alpha - \bar{l}'_F \sin\alpha)/b$ in Equation (5.9) as this is often difficult to predict reliably. The discussion of experimental yaw rate derivatives in Section 3.1 shows that for most conventional configurations the data in Item No. 82010 provide sufficiently accurate estimates of the static fin characteristics for the corrections to be unnecessary. However, if the geometry of the aircraft is such that the interference effects between wing, fin, body and tailplane are more complex than those associated with the comparatively simple arrangements considered in Item No. 82010, then the introduction of the corrections may well prove to be beneficial. The corrections are therefore most likely to be useful for configurations with closely-coupled wings and tailplanes or with body shapes and wing-body junctions that are complicated, such as may be found on high performance fighter aircraft.

TABLE 5.10 Calculation of $(Y_r)_F$, $(N_r)_F$ and $(L_r)_F$

Parameter	Cruise Configuration	Landing Configuration
α	0	6°
M	0.78	0.20
$[(Y_v)_F]_{J_W = 1}$	–0.571	–0.511
$\bar{l}'_F/b$	0.443	0.443
$\bar{z}'_F/b$	0.144	0.144
$(Y_r)_F$	0.253	0.233
$(N_r)_F$	–0.112	–0.106
$(L_r)_F$	0.036	0.023
$(Y_r)_F$ as a function of α	Equation (5.7)	Equation (5.7)
$(N_r)_F$ as a function of α	Equation (5.8)	Equation (5.8)
$(L_r)_F$ as a function of α	Equation (5.9)	Equation (5.9)

## 5.7 Summary of Results and Total Values

The results of the calculations of the various component parts of Y_r, N_r and L_r are summarised in Table 5.11 and illustrated in Sketches 5.5 and 5.6 for the cruise and landing configurations. It can be seen that the fin provides the major contribution to Y_r and N_r and that the fin and wing planform provide the major contributions to L_r, with the deployment of trailing-edge flaps having a large effect on L_r through the planform component.

The variation of the total values of Y_r, N_r and L_r with α and C_L are given in Sketch 5.7 for $M = 0.78$ and in Sketch 5.8 for $M = 0.2$. Both sketches demonstrate that the values of Y_r and N_r only increase slightly in magnitude as α and C_L rise. The values of L_r increase more rapidly initially because they are strongly linked to the wing C_L. The importance of the $(\Delta L_r)_{corr}$ term is clearly visible at high angles of attack. Sketch 5.8 shows that the effect of trailing-edge flap deployment is small for Y_r and N_r but is much more important for L_r, both through the flap lift increment and the flap effect on $(\Delta L_r)_{corr}$. The flap contribution at constant C_L, $(L_r)_f$, is small.

TABLE 5.11 Calculation of Total Values

Parameter		Cruise Configuration		Landing Configuration	
α		0		$6°$	
M		0.78		0.20	
$(Y_r)_B$		–0.053		–0.053	
$(Y_r)_F$		0.253		0.233	
Y_r		0.200		0.180	
$(N_r)_W$ $\begin{cases} N_{r0} \\ N_{rv} \end{cases}$		–0.0017	$\begin{cases} -0.0011 \\ -0.00058 \end{cases}$	–0.0111	$\begin{cases} -0.00094 \\ -0.0102^* \end{cases}$
$(N_r)_f$		–		–0.0030	
$(N_r)_B$		–0.015		–0.015	
$(N_r)_F$		–0.112		–0.106	
N_r		–0.129		–0.135	
$(L_r)_W$ $\begin{cases} (L_r)_p \\ (L_r)_\Gamma \\ (L_r)_\varepsilon \\ (\Delta L_r)_{corr} \end{cases}$		0.0509	$\begin{cases} 0.0606 \\ 0.0066 \\ -0.0103 \\ -0.006 \end{cases}$	0.1874	$\begin{cases} 0.2152^* \\ 0.0049 \\ -0.0077 \\ -0.025 \end{cases}$
$(L_r)_f$		–		–0.0032	
$(L_r)_F$		0.036		0.023	
L_r		0.087		0.207	

*   Including component due to flap lift coefficient increment
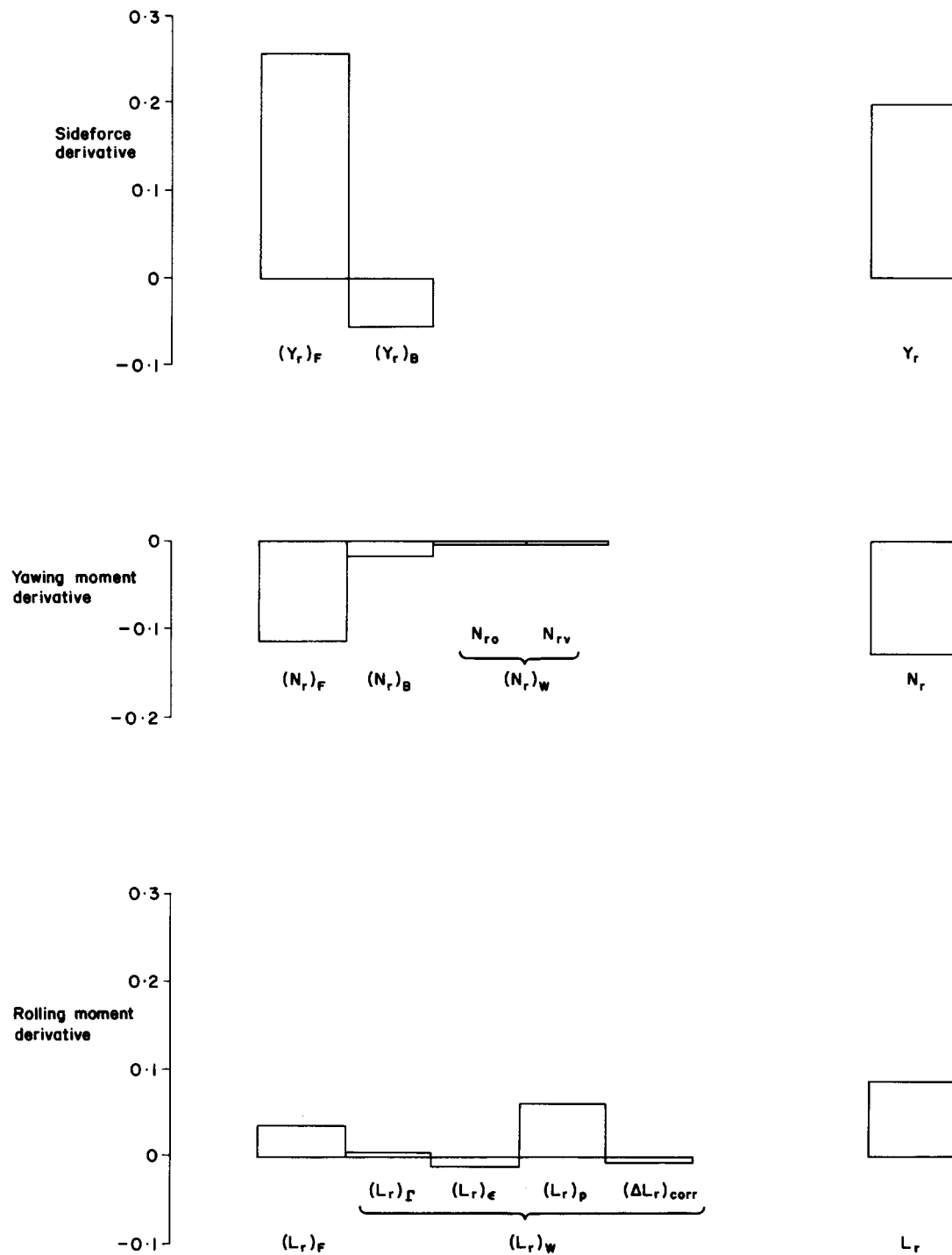
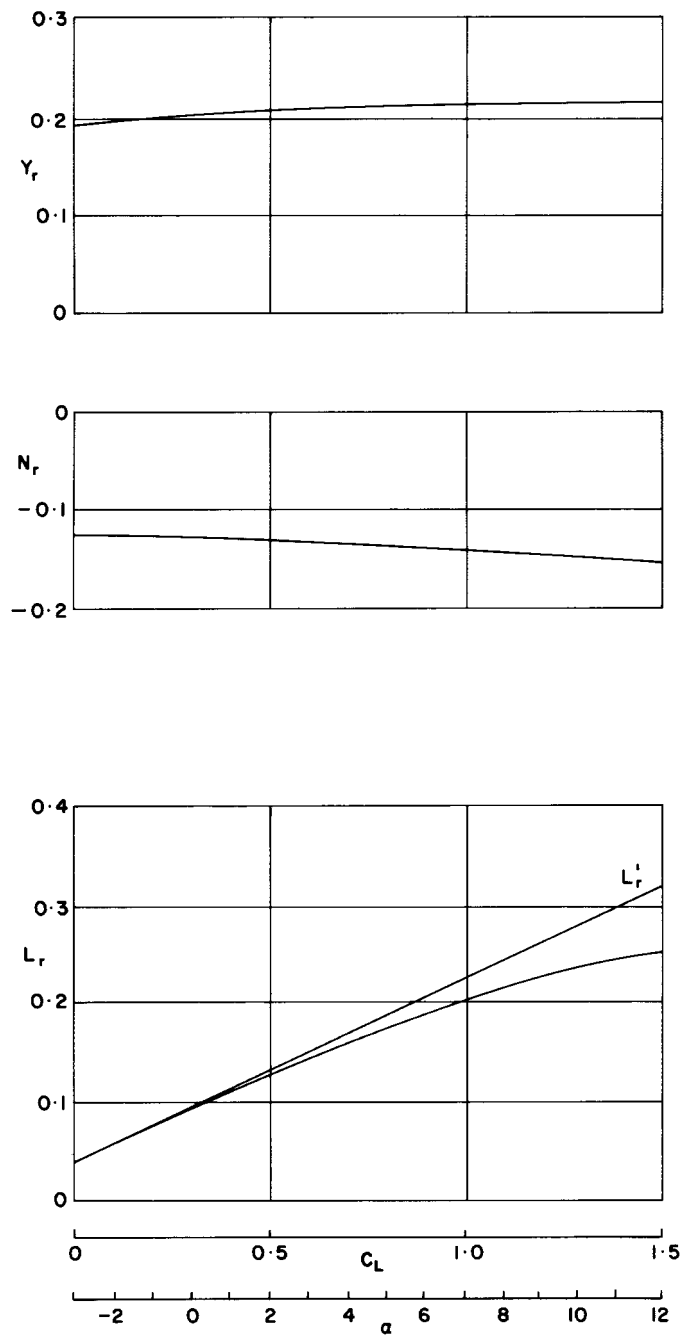**Sketch 5.5 Comparison of components for cruise configuration, $\alpha = 0$**

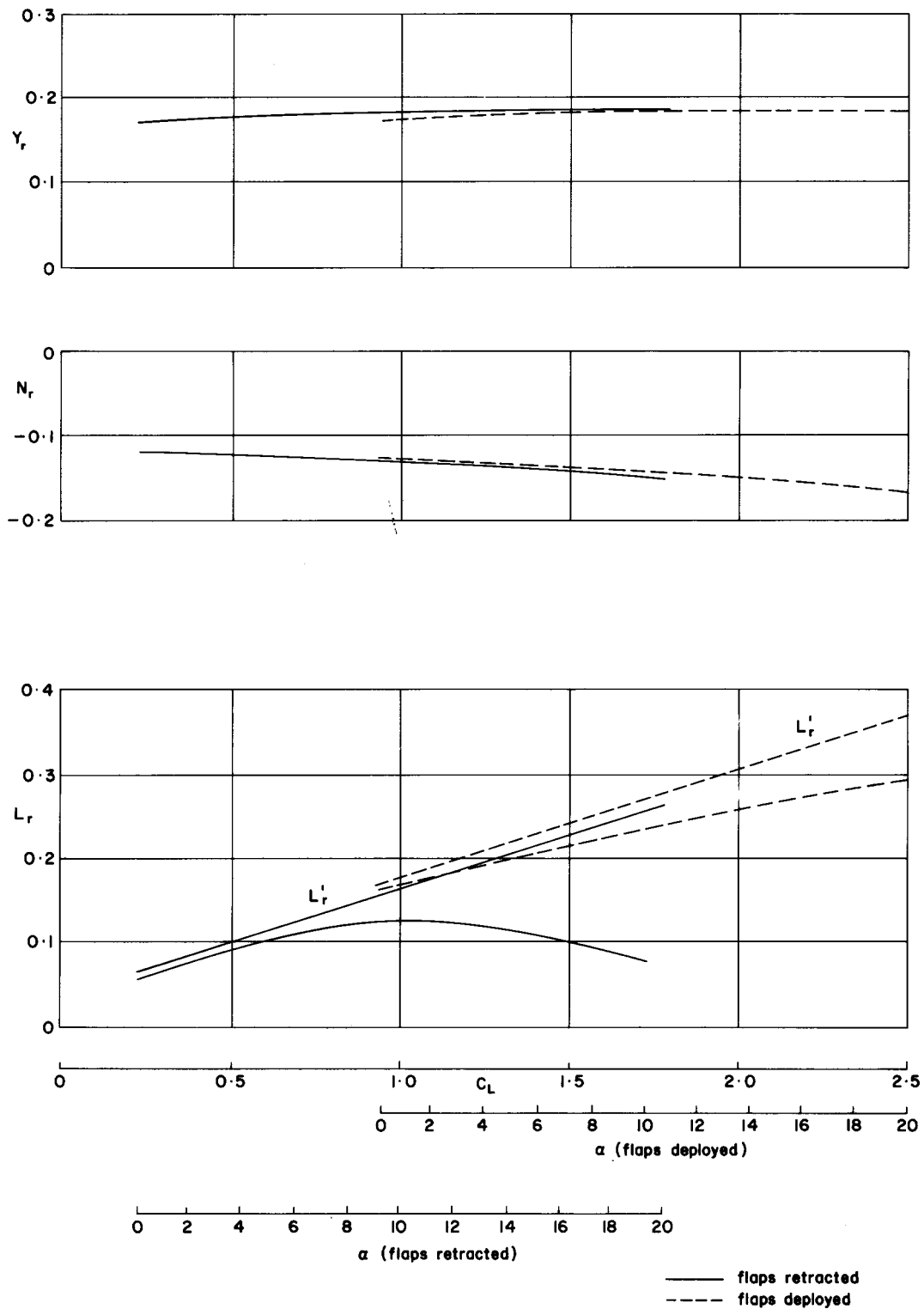**Sketch 5.6   Comparison of components for landing configuration, $\alpha = 6°$**
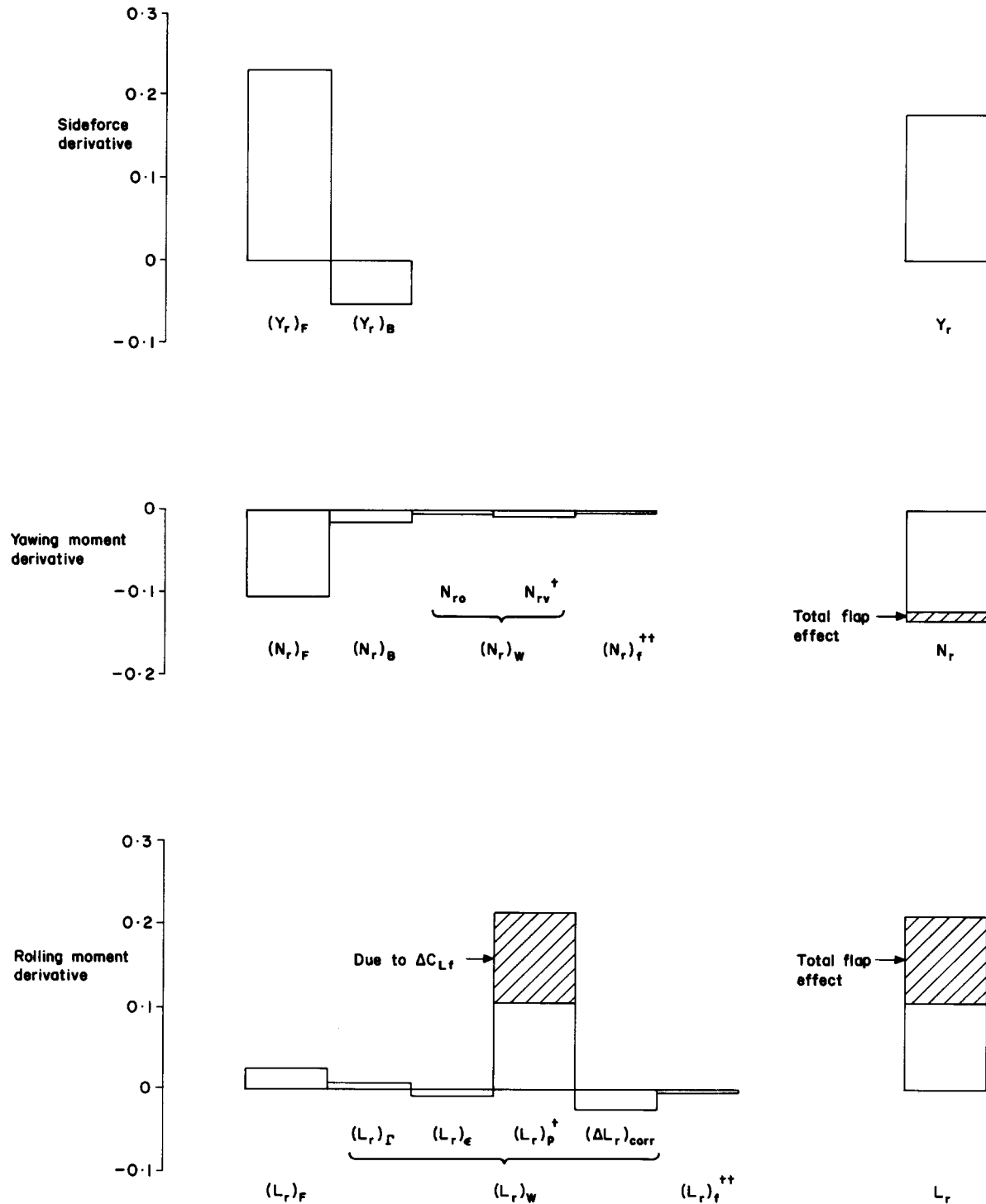
† N_{rv} and $(L_r)_p$ include effect of flap lift coefficient increment

†† $(N_r)_f$ and $(L_r)_f$ are flap contributions at constant C_L

Sketch 5.7   Variation of Y_r **,** N_r **and** L_r **with** α **and** C_L **for** $M = 0.78$

Sketch 5.8   Variation of Y_r, N_r and L_r with α and C_L for $M = 0.2$

APPENDIX A   SIMPLIFIED METHOD

A1.   INTRODUCTION

It is shown in the main text that the fin provides the dominant contribution to Y_r and N_r and that the fin and wing contributions dominate L_r. In the case of the latter it is only the planform contribution $(L_r)_p$ and the correction for partial flow separation $(\Delta L_r)_{corr}$ that are important. (See Sketches 3.8a to 3.8d and Section 5.7.) Advantage of this has been taken to develop a simplified prediction method that is more rapid to apply than the full method, while maintaining a comparable accuracy.

A2.   METHOD

The simplified method has been developed by correlating Y_r against $\overline{l}'_F S_F /bS$, $-N_r$ against $\overline{l}'_F{}^2 S_F /b^2 S$ and $L_r - (L_r)_W$ against $\overline{l}'_F \overline{z}'_F S_F /b^2 S$, where the fin area S_F and the moment arms $\overline{l}'_F$ and $\overline{z}'_F$ may be obtained by inspection of the geometry of interest, see Sketch A2.1, or for a more systematic treatment by applying the methods of Item Nos 82010 and 82017 (Derivations 58 and 60). The correlations are based on low speed, low angle of attack data from curved-flow tests, which are more reliable than oscillatory-rig tests or flight tests, see Section 3.1.) The results for the simplified method are given in Figure A1. The increases in magnitude that accompany a rise in Mach number may be allowed for by multiplying the values in Figure A1 by the ratio of compressible to incompressible flow values of the lift-curve slope of the fin.

The variations of Y_r and N_r with α are sufficiently small to be neglected and, subject to the compressibility factor, their values are obtained directly from Figure A1. The variation of L_r with α is far more significant, and the value of $L_r - (L_r)_W$ at $\alpha = 0$ is multiplied by the ratio $(\overline{z}'_F \cos\alpha - \overline{l}'_F \sin\alpha)/\overline{z}'_F$ to allow for the variation of the rolling moment tail arm. The complete aircraft value is then

$$L_r = [L_r - (L_r)_W]_{\alpha = 0}(\overline{z}'_F \cos\alpha \, - \, \overline{l}'_F \sin\alpha)/\overline{z}'_F + (L_r)_p + (\Delta L_r)_{corr}, \qquad \text{(A2.1)}$$

where $(L_r)_p$ and $(\Delta L_r)_{corr}$ are evaluated as described in Sections 5.4.1 and 5.4.3. If only values at low angles of attack are of interest then $(\Delta L_r)_{corr}$ is small and can be omitted.

The deployment of trailing-edge flaps has a negligible effect on Y_r and N_r. The effect on L_r is important and is allowed for by using the value of C_L appropriate to the wing with flaps deployed when evaluating $(L_r)_p$. The small contribution at constant C_L, $(L_r)_f$, may be neglected.

For some aircraft configurations a simplification of Equation (A2.1) is possible. Reference 64 compares planform contributions to L_r and L_v for a range of wing sweep angles and aspect ratios and shows that to a good approximation $(L_r)_p \approx -0.5(L_v)_p$ provided $30° < \Lambda_{1/4} < 50°$ and $2 < A < 4$. It is also true that for most configurations $\overline{l}'_F \approx 0.5b$, so that $(L_r)_F \approx -0.5(L_v)_F$. For aircraft with geometries satisfying both those criteria, Equation (A2.1) can be rewritten

$$L_r = [L_r - (L_r)_W]_{\alpha = 0} - 0.5(L_{v \; exp} - L_{v0 \; exp}), \qquad \text{(A2.2)}$$

where the experimental values of $L_{v \; exp}$ and $L_{v0 \; exp}$ must be for the complete aircraft in order to include the variation of the fin contribution with α. If high-lift devices are deployed an allowance for their effect is made by taking the value of $L_{v \; exp}$ appropriate to that configuration and the value of $L_{v0 \; exp}$ appropriate to the clean-wing configuration. Equation (A2.2) has the advantage that it does not require any of the

predicted values of L_v that are normally needed in the calculation of $(\Delta L_r)_{corr}$. Comparisons with experimental data for complete aircraft (Derivations 3, 5, 6, 7, 11, 13 and 17) have shown it to be satisfactory. For wings with sweep angles and aspect ratios outside the ranges given above, the simple relationship between $(L_r)_p$ and $(L_v)_p$ becomes increasingly less reliable and Equation (A2.1) must be used.
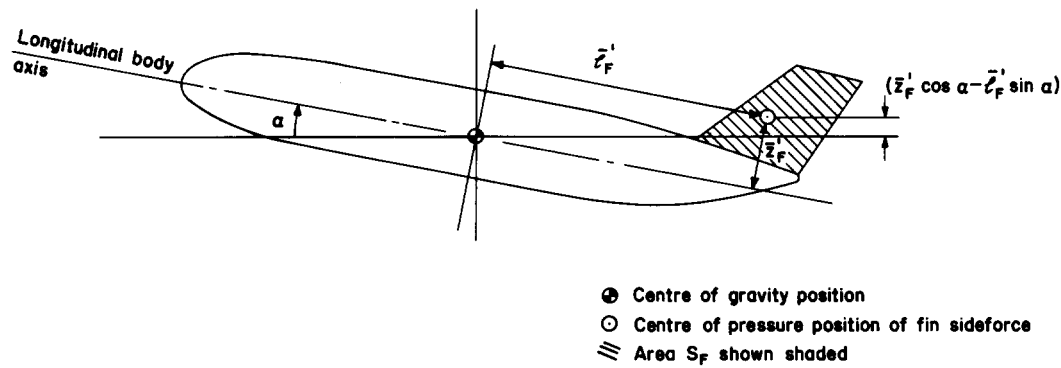
Sketch A2.1

A3. ACCURACY

Comparisons with the experimental data in Derivations 1 to 30 have demonstrated that at low angles of attack the simplified method predicts Y_r, N_r and L_r with an overall accuracy similar to that shown for the full method in Sketches 3.1 to 3.3. However, the simplified method uses direct empirical approximations that form no part of the full method. Therefore, for any particular configuration the predictions of the two methods are independent and may differ within the limits of the overall accuracy. For Y_r and N_r the simplified method gives poorer results if the body contribution is large compared to that of the fin. For L_r both methods are equally reliable throughout the angle of attack range.
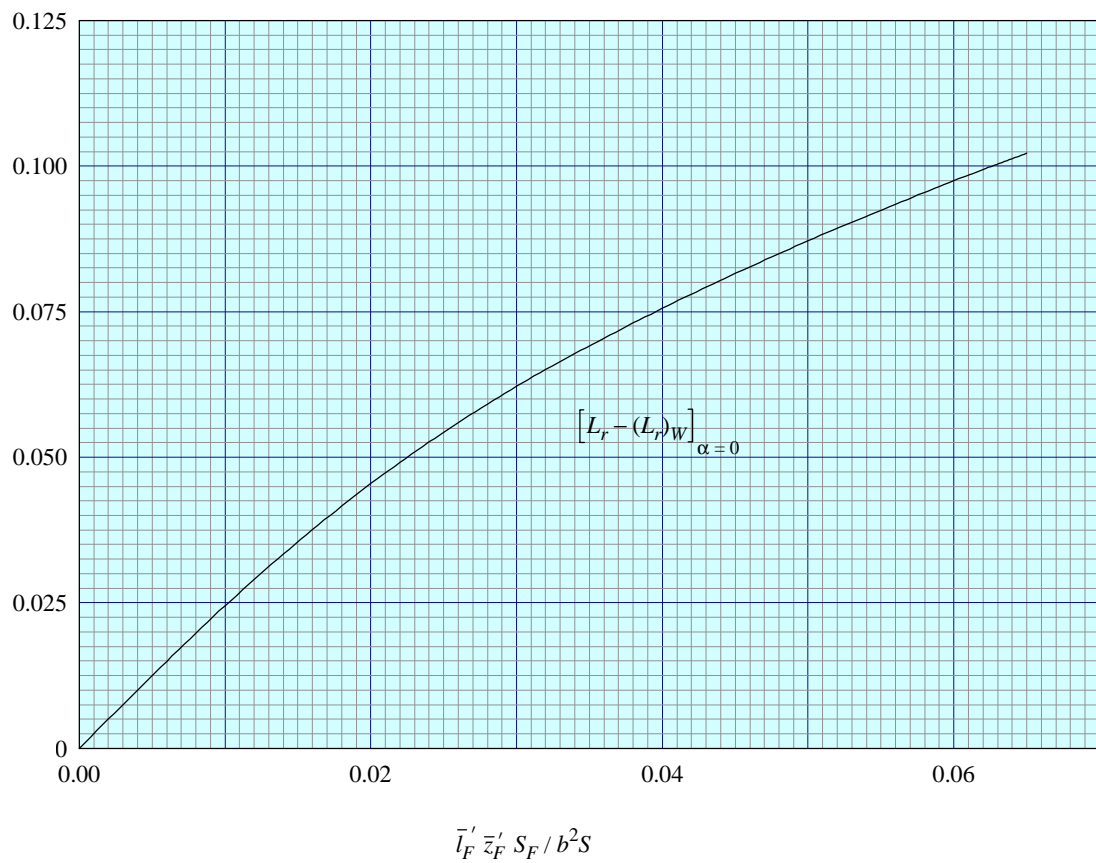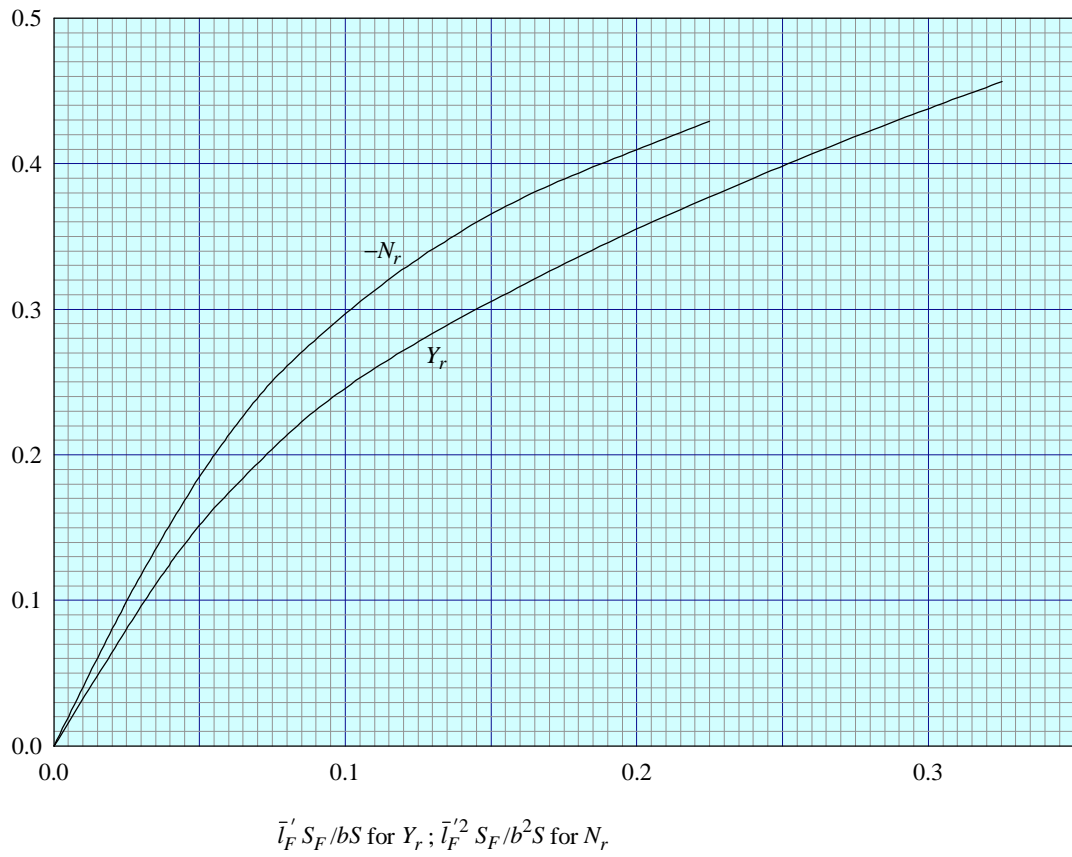
47

$$\bar{l}_F' \, S_F / bS \text{ for } Y_r \, ; \, \bar{l}_F'^2 \, S_F / b^2 S \text{ for } N_r$$

$$\bar{l}_F' \, \bar{z}_F' \, S_F / b^2 S$$

FIGURE A1

THE PREPARATION OF THIS DATA ITEM

The work on this particular Item was monitored and guided by the Aerodynamics Committee which first met in 1942 and now has the following membership:

Chairman
Mr H.C. Garner   – Independent

Vice-Chairman
Mr P.K. Jones   – British Aerospace, Aircraft Group, Manchester

Members
Mr D. Bonenfant   – Aérospatiale, Toulouse, France
Mr E.A. Boyd   – Cranfield Institute of Technology
Mr K. Burgin   – Southampton University
Mr E.C. Carter   – Aircraft Research Association
Mr J.R.J. Dovey   – British Aerospace, Aircraft Group, Warton
Dr J.W. Flower   – Bristol University
Mr A. Hipp   – British Aerospace, Dynamics Group, Stevenage
Mr J. Kloos[*]   – Saab-Scania, Linköping, Sweden
Mr J.R.C. Pedersen   – Independent
Mr I.H. Rettie[*]   – Boeing Aerospace Company, Seattle, Wash., USA
Mr A.E. Sewell[*]   – Northrop Corporation, Hawthorne, Calif., USA
Mr F.W. Stanhope   – Rolls-Royce Ltd, Derby
Mr H. Vogel   – British Aerospace, Aircraft Group, Weybridge
Mr J. Weir   – Salford University.

[*]   Corresponding Member

The member of staff who undertook the technical work involved in the initial assessment of the available information and the construction and subsequent development of the Item was

Mr R.W. Gilbey   – Senior Engineer.